J. Fluid Mech. (2006), *vol.* 552, *pp.* 137–166. © 2006 Cambridge University Press
doi:10.1017/S0022112005008530 Printed in the United Kingdom

Second-order refraction and diffraction of surface water waves

By MENG-YI CHEN AND CHIANG C. MEI

Department of Civil and Environmental Engineering,
Massachusetts Institute of Technology, Cambridge, MA 02139, USA

(Received 6 May 2005 and in revised form 20 September 2005)

The mild-slope equation is an effective approximation for treating the combined effects of refraction and diffraction of infinitesimal water waves, for it reduces the spatial dimension of the linear boundary-value problem from three to two. We extend this approximation to nonlinear waves up to the second order in wave steepness, in order to simplify the inherently three-dimensional task. Assuming that the geometrical complexity is restricted to a finite, though large, horizontal domain, the hybrid-element method designed earlier for linearized problems is modified for the two-dimensional elliptic boundary-value problems at the second order. In the special case of a semi-circular peninsula (or a vertical cylinder on a cliff) in a sea of constant depth, the solution is analytical. Effects of the angle of incidence are examined for the free-surface height along the cylinder. For a cylinder standing on a shoal of radially varying depth, numerical results are discussed.

1. Introduction

The three-dimensional problem of nonlinear diffraction is difficult even for a sea of constant depth bounded by vertical cliff-like coasts. After several earlier attempts, the second-order theory for an axially symmetric body was finally completed by Kim & Yue (1989) who employed a semi-analytical method based on boundary elements. The special case of a vertical circular cylinder was later solved analytically by Chau & Eatock Taylor (1992). Their methods of analysis are fully three-dimensional and have not been extended to nonlinear diffraction and refraction and may be costly if the bathymetry is non-uniform over many wavelengths.

On the other hand, for infinitesimal waves, the combined diffraction and refraction by scatterers over a slowly varying bathymetry can be efficiently analysed by the mild-slope equation (MSE) developed from the linearized theory by Berkhoff (1972). A special advantage of MSE is that it reduces the boundary-value problem from three dimensions to two, and hence facilitates numerical computations involving a large horizontal domain. In the original derivation of Berkhoff (see also Smith & Sprinks (1975) who derived MSE by weighted averaging via Green's formula) terms proportional to the small bed slope ∇h were kept, but those proportional to $(\nabla h)^2$, $\nabla^2 h$ were neglected. For applications to steeper bathymetries, various modifications have been proposed (Kirby 1986; Massel 1993; Chamberlain & Porter 1995; Porter & Staziker 1995; Miles & Chamberlain 1998; Agnon 1999; Athanassoulis & Belibassakis 1999). In particular, Chamberlain & Porter retain the second-order depth-gradient terms and show that the modified mild-slope equation has a better accuracy for scattering by a corrugated seabed of length scale comparable to the surface waves.

https://doi.org/10.1017/S0022112005008530 Published online by Cambridge University Press

Increased accuracy can be achieved for still steeper bed slopes by including all the evanescent modes, leading to an infinite set of two-dimensional modified mild-slope equations coupling all vertical modes (Massel 1993; Porter & Staziker 1995). As far as we are aware, extensions of the mild-slope approximation to nonlinear problems are so far limited to basic ideas, but not yet fully implemented (Agnon 1999).

In coastal dynamics there is a need for the prediction of the diffraction of nonlinear waves over a seabed of depth varying slowly over a large area. Efficient methods that can lighten the computational tasks in three dimensions are required. In this paper, we shall extend the theoretical ideas of the mild-slope approximation to nonlinear diffraction/refraction, so as to simplify the three-dimensional computations. It will be shown that, at second order, the mild-slope equations are a set of two-dimensional coupled elliptic and inhomogeneous partial differential equations with variable coefficients. Application will first be made to the limiting case of a semi-circular cylinder on a wall in a sea of constant depth, for which the equations become uncoupled and the problem is solved analytically. For cases of varying depth, the hybrid-element method of Chen & Mei (1974) for linearized scattering of infinitesimal waves is modified for the inhomogeneous boundary-value problems. A numerical example involving radially varying depth is discussed.

2. Perturbation equations

We assume the fluid to be incompressible and inviscid, and the flow irrotational. Let the velocity field be represented as the gradient of a scalar potential, i.e. $(u, v, w) = \nabla_3 \Phi$. Incompressibility requires that

$$\nabla_3^2 \Phi = \nabla^2 \Phi + \frac{\partial^2 \Phi}{\partial z^2} = 0, \tag{2.1}$$

in the fluid, where ∇ and ∇_3 stand for two- and three-dimensional gradient operators, respectively. For small-amplitude waves, i.e. $\epsilon \equiv kA \ll 1$, where A is the amplitude of the incident waves, we expand the free-surface conditions in powers of $\epsilon \equiv kA$ about $z = 0$, and obtain the approximate dynamic boundary condition,

$$g\zeta + \frac{\partial \Phi}{\partial t} + \zeta \frac{\partial^2 \Phi}{\partial t \partial z} + \tfrac{1}{2} (\nabla_3 \Phi)^2 = O(\epsilon^3), \quad z = 0, \tag{2.2}$$

where ζ denotes the vertical displacement of the free surface. The preceding equation can be combined with the approximate kinematic condition to give,

$$\frac{\partial \Phi}{\partial z} + \frac{1}{g} \frac{\partial^2 \Phi}{\partial t^2} = -\frac{\zeta}{g} \frac{\partial}{\partial z} \left(g \frac{\partial \Phi}{\partial z} + \frac{\partial^2 \Phi}{\partial t^2} \right) - \frac{1}{g} \frac{\partial}{\partial t} (\nabla_3 \Phi)^2 + O(\epsilon^3), \quad z = 0. \tag{2.3}$$

On the seabed, $z = -h(x, y)$, no flux requires that

$$\frac{\partial \Phi}{\partial z} = -\nabla \Phi \cdot \nabla h, \quad z = -h(x, y). \tag{2.4}$$

All lateral boundaries ∂B, including the coast, are assumed to be vertical, so that

$$\frac{\partial \Phi}{\partial n} = \boldsymbol{n} \cdot \nabla \Phi = 0, \quad (x, y) \in \partial B. \tag{2.5}$$

We now introduce the perturbation expansions

$$\Phi = \epsilon \Phi_1 + \epsilon^2 \Phi_2 + \cdots, \quad \zeta = \epsilon \zeta_1 + \epsilon^2 \zeta_2 + \cdots, \tag{2.6}$$

https://doi.org/10.1017/S0022112005008530 Published online by Cambridge University Press

into (2.1) to (2.5). At first and second order, both Φ_1 and Φ_2 satisfy the Laplace equation in the fluid, (2.4) on the sloping seabed, and (2.5) along all lateral boundaries. On the still-water free surface, $z=0$, the boundary condition for the first-order potential is homogeneous

$$g\frac{\partial \Phi_1}{\partial z}+\frac{\partial^2 \Phi_1}{\partial t^2}=0, \quad z=0, \tag{2.7}$$

while that for the second-order potential is not

$$\frac{\partial \Phi_2}{\partial z}+\frac{1}{g}\frac{\partial^2 \Phi_2}{\partial t^2}=\frac{1}{g^2}\frac{\partial \Phi_1}{\partial t}\frac{\partial}{\partial z}\left[g\left(\frac{\partial \Phi_1}{\partial z}\right)+\frac{\partial^2 \Phi_1}{\partial t^2}\right]-\frac{1}{g}\frac{\partial}{\partial t}(\nabla_3 \Phi_1)^2, \quad z=0. \tag{2.8}$$

The free-surface displacement at first order, ζ_1, is related to Φ_1 by

$$\zeta_1=-\frac{1}{g}\left[\frac{\partial \Phi_1}{\partial t}\right]_{z=0}, \tag{2.9}$$

while the second-order correction, ζ_2, consists of two parts,

$$\zeta_2=\zeta_2^{(1)}+\zeta_2^{(2)}. \tag{2.10}$$

One part can be immediately calculated from the first-order solution,

$$\zeta_2^{(1)}=\left[\frac{1}{g^2}\frac{\partial \Phi_1}{\partial t}\frac{\partial^2 \Phi_1}{\partial t\,\partial z}-\frac{1}{2g}(\nabla_3 \Phi_1)^2\right]_{z=0}, \tag{2.11}$$

and the second part depends on the second-order potential Φ_2

$$\zeta_2^{(2)}=\left[-\frac{1}{g}\frac{\partial \Phi_2}{\partial t}\right]_{z=0}, \tag{2.12}$$

whose solution is a major objective of this work.

3. Mild-slope equations

For convenience, we first cite the known result for the first order (Chamberlain & Porter 1995).

3.1. *First-order MSE*

We assume the incident wave to be simple-harmonic in time at first order with the velocity potential

$$\Phi_1=\phi\,\mathrm{e}^{-\mathrm{i}\omega t}+*, \tag{3.1}$$

where * denotes the complex conjugate of the preceding term, and ω the wave frequency.

For vertical lateral boundaries, we take the first-order ϕ to be

$$\phi=-\frac{\mathrm{i}g\eta(x,y)}{\omega}\frac{\cosh k(z+h)}{\cosh kh}, \tag{3.2}$$

where $\eta(x,y)$ is the surface elevation for ω and k is the wavenumber satisfying the dispersion relation

$$\omega^2=gk\tanh kh. \tag{3.3}$$

Since (3.2) representing only the propagating mode is exact for a horizontal seabed, it should be a good approximation for a mildly sloping bed.

https://doi.org/10.1017/S0022112005008530 Published online by Cambridge University Press

By treating Laplace's equation as an ordinary differential equation in z and applying Green's formula (as in Smith & Sprinks 1975), we obtain the modified mild-slope equation for the first-order problem. The result by keeping all terms proportional to ∇h, $\nabla^2 h$ and $(\nabla h)^2$ is the modified mild-slope equation by Chamberlain & Porter (1995),

$$\nabla\cdot(CC_g\nabla\eta)+[k^2CC_g+gU\nabla^2h+gV(\nabla h)^2]\eta=0, \tag{3.4}$$

where

$$U=\frac{(\sinh 2kh-2kh\cosh 2kh)}{4\cosh^2(kh)(2kh+\sinh 2kh)}, \tag{3.5}$$

$$V=\frac{k[(2kh)^4+4(2kh)^3\sinh 2kh-9\sinh 2kh\sinh 4kh]}{12\cosh^2(kh)(2kh+\sinh 2kh)^3} +\frac{k[kh(kh+\sinh 2kh)(\cosh^2 2kh-2\cosh 2kh+3)]}{\cosh^2(kh)(2kh+\sinh 2kh)^3}, \tag{3.6}$$

C is the phase velocity

$$C=\frac{\omega}{k}, \tag{3.7}$$

and C_g is the group velocity,

$$C_g=\frac{C}{2}\left(1+\frac{2kh}{\sinh 2kh}\right). \tag{3.8}$$

Note that while no terms related to the gradients of depth are omitted, the assumed potential (3.2) is not exact and does not satisfy the bottom condition. The above approximation is therefore still restricted to mild slope.

Equation (3.4) with the appropriate radiation condition can be solved numerically by the hybrid element method of Chen & Mei (1974) if the complex geometry is limited to a finite near field. Afterwards, the first-order free-surface elevation is given by

$$\zeta_1=\eta e^{-i\omega t}+*. \tag{3.9}$$

With these results, the following part of the second-order free-surface displacement can be computed immediately,

$$\zeta_2^{(1)}=\eta_{2,0}^{(1)}+\left(\eta_{2,2}^{(1)}e^{-i2\omega t}+*\right). \tag{3.10}$$

In particular, $\eta_{2,0}^{(1)}$ represents the mean sea-level set-up/setdown

$$\eta_{2,0}^{(1)}=\frac{\omega^2}{g}|\eta|^2-\frac{g}{\omega^2}|\nabla\eta|^2, \tag{3.11}$$

and $\eta_{2,2}^{(1)}$ represents the second-harmonic amplitude due directly to quadratic interactions of the first-order motion

$$\eta_{2,2}^{(1)}=\frac{3\omega^2}{2g}\eta^2+\frac{g}{2\omega^2}(\nabla\eta)^2. \tag{3.12}$$

Solution of the remaining second harmonic,

$$\zeta_2^{(2)}=\eta_{22}^{(2)}e^{-2i\omega t}+*, \tag{3.13}$$

must await the solution of Φ_2.

https://doi.org/10.1017/S0022112005008530 Published online by Cambridge University Press

3.2. *Second-order MSE*

At second-order, the inhomogeneous free-surface boundary condition, (2.8), can be rewritten as follows

$$\frac{\partial \Phi_2}{\partial z} + \frac{1}{g}\frac{\partial^2 \Phi_2}{\partial t^2} = F\mathrm{e}^{-2\mathrm{i}\omega t} + *, \tag{3.14}$$

where

$$F = \widehat{\beta}\eta\eta + \bar{\beta}\nabla\eta\cdot\nabla\eta, \tag{3.15}$$

with

$$\widehat{\beta} = \frac{\mathrm{i}gk^2}{\omega} - \frac{3\mathrm{i}\omega^3}{g}, \quad \bar{\beta} = -\frac{2\mathrm{i}g}{\omega}. \tag{3.16}$$

Expressing the second-order potential in the form

$$\Phi_2 = \psi\mathrm{e}^{-2\mathrm{i}\omega t} + *, \tag{3.17}$$

it is easy to see that ψ must satisfy $\partial\psi/\partial n = 0$ along lateral boundaries, (2.4) on the seabed and

$$\frac{\partial \psi}{\partial z} - \frac{4\omega^2}{g}\psi = F, \quad z = 0 \tag{3.18}$$

on the free surface.

Similar to the first-order mild-slope approximation of Porter & Staziker (1995), we express the solution for ψ as the sum of all vertical eigenmodes in a sea of constant depth

$$\psi = -\frac{\mathrm{i}g}{2\omega}\sum_{\ell=0}^{\infty}\xi_\ell\frac{\cos\kappa_\ell(z+h)}{\cos\kappa_\ell h}, \tag{3.19}$$

where κ_ℓ, $\ell = 1, 2, \ldots$ are the real roots of the transcendental equation

$$-4\omega^2 = g\kappa_\ell\tan\kappa_\ell h, \quad \left(\ell - \tfrac{1}{2}\right)\pi \leqslant \kappa_\ell h \leqslant \ell\pi, \tag{3.20}$$

and $\kappa_0 = -\mathrm{i}\widehat{\kappa}_0$ is imaginary with $\widehat{\kappa}_0$ being the real root of the dispersion equation

$$4\omega^2 = g\widehat{\kappa}_0\tanh\widehat{\kappa}_0 h. \tag{3.21}$$

Physically, the term with the subscript $m = 0$ corresponds to the propagating mode while those with $m \geqslant 1$ correspond to the evanescent modes. Because of the inhomogeneous condition (3.18) on the free surface, all vertical modes are required, unlike the first-order potential in (3.2). Employing the procedure of weighted vertical averaging via Green's formula, as outlined in Appendix A, we obtain a matrix equation coupling all second-order modal amplitudes ξ_ℓ:

$$\sum_{\ell=0}^{\infty}\{\nabla\cdot(A_{m,\ell}\nabla\xi_\ell) + B_{m,\ell}\nabla h\cdot\nabla\xi_\ell + C_{m,\ell}\xi_\ell\} = -\mathrm{i}2\omega F, \quad m = 0, 1, 2, 3, \ldots. \tag{3.22}$$

The coefficient matrices defined below are functions of (x, y),

$$A_{m,\ell} = \delta_{m\ell}A_{\ell,\ell} = \frac{gh}{2\cos^2\kappa_\ell h}\left(1 + \frac{\sin 2\kappa_\ell h}{2\kappa_\ell h}\right)\delta_{m\ell}, \tag{3.23}$$

$$B_{m,\ell} = \begin{cases} 0 & \text{for } m = \ell, \\ g(U_{m,\ell} - U_{\ell,m}) & \text{for } m \neq \ell, \end{cases} \tag{3.24}$$

https://doi.org/10.1017/S0022112005008530 Published online by Cambridge University Press

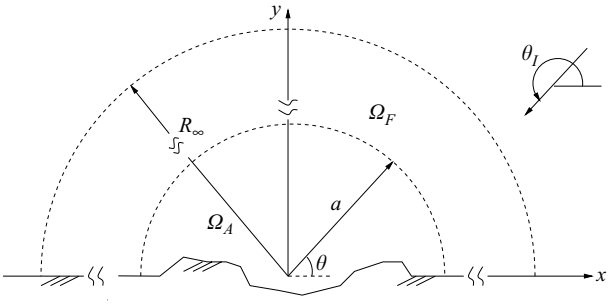


FIGURE 1. Near (Ω_A) and far (Ω_F) fields. Variable bathymetry and non-straight coastal boundaries are in (Ω_A) behind the semi-circle $r = a$.

with

$$U_{m,\ell} = \begin{cases} \dfrac{\sin 2\kappa_m h - 2\kappa_m h \cos 2\kappa_m h}{4\cos^2(\kappa_m h)\,(2\kappa_m h + \sin 2\kappa_m h)} & \text{if } m = \ell, \\ -\dfrac{\kappa_\ell^2}{\cos\kappa_m h \cos\kappa_\ell h \left(\kappa_\ell^2 - \kappa_m^2\right)}, & \text{if } m \neq \ell, \end{cases} \tag{3.25}$$

$$C_{m,\ell} = -\kappa_m^2 A_{m,\ell} + g U_{m,\ell} \nabla^2 h + g V_{m,\ell} (\nabla h)^2, \tag{3.26}$$

with

$$V_{m,m} = \frac{\kappa_m[-(2\kappa_m h)^4 - 4(2\kappa_m h)^3 \sin 2\kappa_m h - 9\sin(2\kappa_m h)\sin 4\kappa_m h]}{12\cos^2(\kappa_m h)(2\kappa_m h + \sin 2\kappa_m h)^3} + \frac{\kappa_m[\kappa_m h(\kappa_m h + \sin 2\kappa_m h)(\cos^2 2\kappa_m h - 2\cos 2\kappa_m h + 3)]}{\cos^2(\kappa_m h)(2\kappa_m h + \sin 2\kappa_m h)^3} \tag{3.27}$$

for $m = \ell$, and

$$V_{m,\ell} = \frac{-2\kappa_\ell \sec\kappa_m h \sec\kappa_\ell h}{(2\kappa_\ell h + \sin 2\kappa_\ell h)} \frac{\left[4\kappa_\ell^2\kappa_m^2 + \left(\kappa_\ell^4 - \kappa_m^4\right)\sin^2\kappa_\ell h\right]}{\left(\kappa_\ell^2 - \kappa_m^2\right)^2} \tag{3.28}$$

for $m \neq \ell$. These coefficients are equivalent to those in the modified system of mild-slope equations of Porter & Staziker (1995) for linearized waves and $F = 0$, after changing 2ω to ω. We have now reduced the second-order task to the solution of coupled two-dimensional elliptic problems, subject to certain boundary conditions.

In the region of constant depth, terms multiplied by $B_{m\ell}$ vanish, while $C_{m,\ell}$ is also a diagonal matrix. Equations (3.22) are no longer coupled and reduce to

$$\nabla^2\xi_\ell - \kappa_\ell^2\xi_\ell = -\mathrm{i}\frac{2\omega}{A_{\ell,\ell}}F, \quad \ell = 0, 1, 2, \ldots. \tag{3.29}$$

For coastal waters where only the complexities of local topography and coastline are of major concern, we can simplify the geometry in areas far from the local region. With reference to figure 1, let us divide the horizontal fluid domain into two regions : the near field Ω_A in which the bathymetry and coastal boundary are complex, and the far field Ω_F where the depth is constant and the coastline straight. The two fields are separated by a semi-circle ∂A of radius $r = a$. For the first-order problem, the far-field solution in Ω_F can be represented analytically as an eigenfunction expansion. In the near field Ω_A, discrete solutions will be sought via finite elements. The unknown nodal coefficients in Ω_A and the expansion coefficients in Ω_F will be found together

https://doi.org/10.1017/S0022112005008530 Published online by Cambridge University Press

by Galerkin's method, subject to the continuity of η and $\partial\eta/\partial r$ at $r=a$. This is the idea of the hybrid-element method developed for linearized wave problems by Chen & Mei (1974) and Bai & Yeung (1974) for two dimensions and Yue, Chen & Mei (1978) for three dimensions. The method will be extended to the second-order problem here with the requirement of continuity of ξ_ℓ and $\partial\xi_\ell/\partial r$ at $r=a$.

4. Analytical representations in the far field

As a part of the hybrid-element analysis, let us first present the analytical representations in the far field Ω_F where the depth is constant and the coastline is along the x-axis.

4.1. *First order*

In the far field, the first-order wave consists of the incident, reflected and scattered waves given together by

$$(\eta)_{\Omega_F} = \eta^{(T)} + \eta^{(S)}, \tag{4.1}$$

where

$$\eta^{(T)} = \tfrac{1}{2}A\exp(\mathrm{i}kr\cos(\theta-\theta_I)) + \tfrac{1}{2}A\exp(\mathrm{i}kr\cos(\theta+\theta_I)). \tag{4.2}$$

is the sum of incident and reflected waves in the presence of the straight coast, with θ_I being the incidence angle. The first-order scattered wave $\eta^{(S)}$ is formally

$$\eta^{(S)} = \sum_{m=0}^{\infty} \epsilon_m \mathrm{i}^m \alpha_m H_m(kr)\cos m\theta, \tag{4.3}$$

where ϵ_m is the Jacobi symbol, being 1 for $m=0$ and 2 for $m=1,2,3,\ldots$, $H_m(kr)\equiv H_m^{(1)}(kr)$ is a Hankel function of the first kind, and the coefficients $\alpha_m, m=0,1,2,\ldots$, are as yet unknown.

In the near field of complex bathymetry and coastline, discrete finite elements are used. The coupled problems of near and far fields are solved numerically via a variational principle as in Chen & Mei (1974) as described by Houston (1981). Afterwards the nodal values of η in the near field and the coefficients α_m of the far field are found.

4.2. *Second order*

4.2.1. *The forcing function F*

Referring to (3.15), F contains quadratic products of the first-order waves and can be decomposed as follows

$$F = \mathscr{P} + \mathscr{Q} \tag{4.4}$$

where $\mathscr{P}$ denotes the part associated with the self- and cross-interactions of progressive waves (incident and reflected waves),

$$\mathscr{P} = \widehat{\beta}\eta^{(T)}\eta^{(T)} + \bar{\beta}\nabla\eta^{(T)}\cdot\nabla\eta^{(T)}, \tag{4.5}$$

and

$$\mathscr{Q} = \widehat{\beta}\left[2\eta^{(T)}+\eta^{(S)}\right]\eta^{(S)} + \bar{\beta}\left[2\nabla\eta^{(T)}+\nabla\eta^{(S)}\right]\cdot\nabla\eta^{(S)} \tag{4.6}$$

is the part due to cross-interactions between the plane progressive waves and the scattered waves, and the self-interaction of the scattered waves.

By straightforward calculations, we obtain

$$\begin{aligned}\mathscr{P} = \mathscr{M}+\mathscr{N} = {} & \tfrac{1}{4}A^2(\widehat{\beta}-\bar{\beta}k^2)[\exp(\mathrm{i}2kr\cos(\theta-\theta_I)) + \exp(\mathrm{i}2kr\cos(\theta+\theta_I))] \\ & + \tfrac{1}{2}A^2[\widehat{\beta}-\bar{\beta}k^2\cos(2\theta_I)]\exp(\mathrm{i}2kr\cos\theta_I\cos\theta).\end{aligned} \tag{4.7}$$

https://doi.org/10.1017/S0022112005008530 Published online by Cambridge University Press

Clearly, the first line,

$$\mathscr{M} = \tfrac{1}{4}A^2(\widehat{\beta} - \bar{\beta}k^2)[\exp(\mathrm{i}2kr\cos(\theta - \theta_I)) + \exp(\mathrm{i}2kr\cos(\theta + \theta_I))], \tag{4.8}$$

represents a pair of obliquely incident and reflected plane waves of wavenumber $2k$, and the second line,

$$\mathscr{N} = \tfrac{1}{2}A^2[\widehat{\beta} - \bar{\beta}k^2\cos(2\theta_I)]\exp(\mathrm{i}2kr\cos\theta_I\cos\theta), \tag{4.9}$$

is a plane incident wave of wavenumber $2k\cos\theta_I$ propagating along the coastline.

To calculate the forcing function $\mathscr{Q}$, we first represent the first-order progressive wave as a partial wave expansion

$$\eta^{(T)} = \sum_{m=-\infty}^{\infty} T_m \mathrm{e}^{(\mathrm{i}m\theta)} \text{ with } T_m(r) = A\mathrm{i}^m J_m(kr)\cos m\theta_I, \tag{4.10}$$

and the first-order scattered waves as

$$\eta^{(S)} = \sum_{m=-\infty}^{\infty} S_m \mathrm{e}^{\mathrm{i}m\theta} \quad \text{where } S_m(r) = \mathrm{i}^m \alpha_m H_m(kr) \tag{4.11}$$

where the coefficients α_m are to be solved by the hybrid-element method. Because of the no flux condition on the straight coast,

$$\frac{1}{r}\frac{\partial\left(\eta^{(T)}, \eta^{(S)}\right)}{\partial\theta} = 0, \quad \theta = 0, \pi, \tag{4.12}$$

α_m, T_m, S_m must be even in m.

We now calculate $\mathscr{Q}$ according to (4.6). A typical cross-product in (4.6) is of the form

$$\eta^{(T)}\eta^{(S)} = \sum_{m=-\infty}^{\infty} T_m \mathrm{e}^{\mathrm{i}m\theta} \sum_{n=-\infty}^{\infty} S_n \mathrm{e}^{\mathrm{i}n\theta} = \sum_{m=-\infty}^{\infty}\left[\sum_{n=-\infty}^{\infty} T_{m-n}S_n\right]\mathrm{e}^{\mathrm{i}m\theta}. \tag{4.13}$$

It follows that $\mathscr{Q}$ can be expressed as a Fourier series

$$\mathscr{Q} = \sum_{m=-\infty}^{\infty} \mathscr{Q}_m \mathrm{e}^{\mathrm{i}m\theta} = \sum_{m=0}^{\infty} \epsilon_m \mathscr{Q}_m(r)\cos m\theta, \tag{4.14}$$

with

$$\mathscr{Q}_m = \sum_{n=-\infty}^{\infty}\left\{\left[\widehat{\beta} - \frac{n(m-n)}{r^2}\bar{\beta}\right]S_n(2T_{m-n} + S_{m-n}) + \bar{\beta}\frac{\partial S_n}{\partial r}\left(2\frac{\partial T_{m-n}}{\partial r} + \frac{\partial S_{m-n}}{\partial r}\right)\right\}. \tag{4.15}$$

4.2.2. *Decomposition of the far-field solution*

In accordance with the form of the forcing term, the second-order response $(\xi_\ell)_{\Omega_F}$ defined by (3.19) can be separated into three parts,

$$(\xi_\ell)_{\Omega_F} = \xi_\ell^P + \xi_\ell^Q + \xi_\ell^H. \tag{4.16}$$

The first part, ξ_ℓ^P, is the direct response to $\mathscr{P}$. Thus, it satisfies the following inhomogeneous equation

$$\left(\nabla^2 - \kappa_\ell^2\right)\xi_\ell^P = -\mathrm{i}\frac{2\omega\mathscr{P}}{A_{\ell,\ell}}, \quad \ell = 0, 1, 2, 3, \ldots. \tag{4.17}$$

The above decomposition is not unique. It will be shown in the next subsection that the solution is just the sum of three Stokes' waves.

https://doi.org/10.1017/S0022112005008530 Published online by Cambridge University Press

The second part, ξ_ℓ^Q, is the response to forcing by $\mathscr{Q}$ and is required to satisfy the inhomogeneous equation

$$\left(\nabla^2 - \kappa_\ell^2\right)\xi_\ell^Q = -\mathrm{i}\frac{2\omega\mathscr{Q}}{A_{\ell,\ell}}, \quad \ell = 0, 1, 2, 3, \ldots, \tag{4.18}$$

the no-flux condition along the straight coast

$$\frac{\partial \xi_\ell^Q}{\partial \theta} = 0, \quad r > a; \quad \theta = 0, \quad \theta = \pi, \quad \ell = 0, 1, 2, 3, \ldots, \tag{4.19}$$

and along the semi-circle $r = a$

$$\frac{\partial \xi_\ell^Q}{\partial r} = 0, \quad r = a, \quad 0 \leqslant \theta \leqslant \pi, \quad \ell = 0, 1, 2, 3, \ldots. \tag{4.20}$$

This condition is chosen for convenience. For the evanescent modes, $\ell = 1, 2, 3, \ldots$, ξ_ℓ^Q diminishes to zero at large enough r. For the propagating mode, $\ell = 0$, ξ_0^Q must satisfy the weak (integral) radiation condition at infinity owing to the slow attenuation of Q. We shall call both ξ_ℓ^P and ξ_ℓ^Q the *forced waves*.

Finally, ξ_ℓ^H is the solution to the homogeneous Helmholtz equation

$$\left(\nabla^2 - \kappa_\ell^2\right)\xi_\ell^H = 0, \quad \ell = 0, 1, 2, 3, \ldots, \tag{4.21}$$

and the no-flux condition along the straight coast,

$$\frac{\partial \xi_\ell^H}{\partial \theta} = 0, \quad r > a, \quad \theta = 0 \quad \theta = \pi, \quad \ell = 0, 1, 2, 3, \ldots. \tag{4.22}$$

In addition, ξ_ℓ^H must satisfy the usual (strong) radiation condition at infinity. To be referred to as the *free wave*, the formal solution ξ_ℓ^H is immediate

$$\xi_\ell^H = \sum_{m=0}^{\infty} \epsilon_m \widehat{\alpha}_{\ell,m} K_m(\kappa_\ell r)\cos m\theta, \quad \ell = 0, 1, 2, 3, \ldots, \tag{4.23}$$

where K_m is the modified Bessel function of the second kind of order m. For $\ell = 0$, $\kappa_0 = -\mathrm{i}\widehat{\kappa}_0$ is imaginary and $K_m(\kappa_0 r)$ is proportional to $H_m^{(1)}(\widehat{\kappa}_0 r)$. The unknown coefficients $\widehat{\alpha}_{\ell,m}$ will be found jointly with the discrete solution in the near field by the hybrid-element analysis to be described shortly, which requires the continuity of potentials and their radial derivatives along $r = a$.

The solutions for ξ_ℓ^P and ξ_ℓ^Q can be obtained explicitly, as shown below.

4.2.3. *Response ξ_ℓ^P to forcing $\mathscr{P}$ by progressive waves*

It is easy to derive from (4.17) that

$$\xi_\ell^P = \xi_\ell^I + \xi_\ell^R + \xi_\ell^{IR}, \quad \ell = 0, 1, 2, 3, \ldots \tag{4.24}$$

where

$$\begin{aligned} \xi_\ell^I &= L_\ell^M \exp(\mathrm{i}2kr\cos(\theta - \theta_I)), \quad \xi_\ell^R = L_\ell^M \exp(\mathrm{i}2kr\cos(\theta + \theta_I)), \\ \xi_\ell^{IR} &= L_\ell^N \exp(\mathrm{i}2kr\cos\theta_I\cos\theta), \end{aligned} \tag{4.25}$$

with

$$L_\ell^M = \frac{2\mathrm{i}\omega}{A_{\ell,\ell}}\frac{A^2}{4}\frac{(\widehat{\beta} - \bar{\beta}k^2)}{4k^2 + \kappa_\ell^2}, \quad L_\ell^N = \frac{2\mathrm{i}\omega}{A_{\ell,\ell}}\frac{A^2}{2}\frac{[\widehat{\beta} - \bar{\beta}k^2\cos(2\theta_I)]}{(2k\cos\theta_I)^2 + \kappa_\ell^2}. \tag{4.26}$$

https://doi.org/10.1017/S0022112005008530 Published online by Cambridge University Press

Substituting (4.25) into (3.19), we obtain the corresponding second-order potentials Φ_2^I, Φ_2^R and Φ_2^{IR},

$$\begin{pmatrix}\Phi_2^I\\ \Phi_2^R\end{pmatrix} = \left[\sum_{\ell=0}^{\infty} \frac{g}{A_{\ell,\ell}\left(4k^2+\kappa_\ell^2\right)} \frac{\cos\kappa_\ell(z+h)}{\cos\kappa_\ell h}\right] \times (\widehat{\beta}-\bar{\beta}k^2)\frac{A^2}{4}\exp(\mathrm{i}2kr\cos(\theta\mp\theta_I)-\mathrm{i}2\omega t)+*, \tag{4.27}$$

and

$$\Phi_2^{IR} = \left[\sum_{\ell=0}^{\infty} \frac{g}{A_{\ell,\ell}\left((2k\cos\theta_I)^2+\kappa_\ell^2\right)} \frac{\cos\kappa_\ell(z+h)}{\cos\kappa_\ell h}\right] \times (\widehat{\beta}-\bar{\beta}k^2\cos 2\theta_I)\frac{A^2}{2}\exp(\mathrm{i}2kr\cos\theta_I\cos\theta-\mathrm{i}2\omega t)+*. \tag{4.28}$$

For normal incidence $\theta_I = 3\pi/2$, the second-harmonic potential Φ_2^{IR} becomes independent of (x, y, z) (or r, θ, z); the associated second harmonic pressure persists for all depth down to the seabed and can induce microseisms, as shown first by Longuet-Higgins (1950) for a pure standing wave in deep water on a straight coast.

In Appendix B, it is shown that Φ_2^I, Φ_2^R and Φ_2^{IR} are just the series expansions of the second-order part of the classical Stokes waves. (Strictly speaking, the classical Stokes wave is a single wave train. The three-term result here is the second-order part of an obliquely incident and reflected wave system.) While the Stokes forms are more compact, the series forms here are more convenient for later computations.

4.2.4. *Response $\xi_\ell^{\mathcal{Q}}$ to forcing by $\mathcal{Q}$*

To solve the inhomogeneous problem for each $\xi_\ell^{\mathcal{Q}}$, we shall employ two-dimensional Green's functions, $G_\ell(r, \theta; r_0, \theta_0)$, described in Appendix C. By Green's theorem, the boundary conditions and the reciprocity of Green's functions, we find at any field point (r, θ),

$$\xi_\ell^{\mathcal{Q}}(r,\theta) = \int_a^\infty r_0\,\mathrm{d}r_0 \int_0^\pi \mathrm{d}\theta_0 \left[-\mathrm{i}\frac{2\omega\mathcal{Q}(r_0,\theta_0)}{A_{\ell,\ell}}\right] \sum_{m=0}^{\infty} \frac{\epsilon_m}{\pi}\cos m\theta\cos m\theta_0 K_m(\kappa_\ell r_>) \times \left[\frac{I_m'(\kappa_\ell a)}{K_m'(\kappa_\ell a)}K_m(\kappa_\ell r_<) - I_m(\kappa_\ell r_<)\right], \quad \ell = 0, 1, 2, 3, \ldots. \tag{4.29}$$

where

$$r_< = \min(r, r_0), \quad r_> = \max(r, r_0). \tag{4.30}$$

The series above is the Green function $G_\ell(r, \theta; r_0, \theta_0)$. Use has been made of the facts that (i) for $\ell = 1, 2, 3, \ldots$, the evanescent modes die out exponentially at infinity, and (ii) for $\ell = 0$, the propagating mode satisfies the weak radiation condition, i.e. the integral below vanishes in the limit of large r,

$$\int_{\partial\Omega_\infty}\left(\xi_0\frac{\partial G_0}{\partial n} - G_0\frac{\partial\xi_0}{\partial n}\right)\mathrm{d}S = O\left(\frac{1}{\sqrt{r}}\right)\to 0, \quad r\to\infty. \tag{4.31}$$

Verification of this result is similar to that given in Mei (1989, p. 664). Using the Fourier expansion (4.14) for $\mathcal{Q}(r, \theta)$, the orthogonality of cosines, and the Wronskian

https://doi.org/10.1017/S0022112005008530 Published online by Cambridge University Press

identity of Bessel functions, we obtain the value on the circle $r=a$,

$$\xi_\ell^Q(a,\theta)=\sum_{m=0}^{\infty}\frac{\epsilon_m}{\kappa_\ell a}\cos(m\theta)\int_a^\infty r_0\,\mathrm{d}r_0\left[-\mathrm{i}\frac{2\omega\mathscr{Q}_m(r_0)}{A_{\ell,\ell}}\right]\frac{K_m(\kappa_\ell r_0)}{K_m'(\kappa_\ell a)},\quad \ell=0,1,2,3,\ldots, \tag{4.32}$$

which is needed to calculate the finite-element solution inside Ω_A. The numerical evaluation of the integral above can be expedited by the scheme of Chau & Eatock Taylor (1992).

In summary, the second-order solution in the far-field is known analytically except for the unknown coefficients $\widehat{\alpha}_{\ell,m}$ of the second-order free wave.

5. Hybrid-element solution

In the near field Ω_A of complex geometry, the amplitudes $\xi_\ell(x,y)$ (without decomposition) satisfy (3.22) where the forcing function $F(x,y)$ is known at every nodal point from the numerical solution of the first-order problem. The no-flux condition must be imposed on the lateral boundary ∂B which is the union of the complex coastline (peninsula etc.),

$$\left(\frac{\partial\xi_\ell}{\partial n}\right)_{\Omega_A}=0\quad\text{on }\partial B,\quad \ell=0,1,2,3,\ldots, \tag{5.1}$$

In addition we require the continuity of pressure along and flux across the semi-circle $\partial A:(r=a,0\leqslant\theta\leqslant\pi)$

$$(\xi_\ell)_{\Omega_A}=\xi_\ell^P+\xi_\ell^Q+\xi_\ell^H,\quad r=a,\quad \ell=0,1,2,3,\ldots, \tag{5.2}$$

$$\left(\frac{\partial\xi_\ell}{\partial r}\right)_{\Omega_A}=\frac{\partial\xi_\ell^P}{\partial r}+\frac{\partial\xi_\ell^H}{\partial r},\quad r=a,\quad \ell=0,1,2,3,\ldots. \tag{5.3}$$

Use has been made of (4.20). These conditions are imposed on the nodal points along the semicircle. Recall that the far-field solutions ξ_ℓ^P, ξ_ℓ^Q and ξ_ℓ^H are given by (4.24), (4.32) and (4.23), the last of which still contains the unknown coefficients $\widehat{\alpha}_{\ell,m}$.

5.1. *Finite-element analysis*

Equation (3.22) is first truncated after a finite number of $N_\xi+1$ modes; that is, $(\ell,m)=0,1,\ldots,N_\xi$. Afterwards we applied the method of weighted residuals and form the integrals for the truncated equation

$$\iint_{\Omega_A}\left\{-\sum_{\ell=0}^{N_\xi}[\nabla\cdot(A_{m,\ell}\nabla\xi_\ell)+B_{m,\ell}\nabla h\cdot\nabla\xi_\ell+C_{m,\ell}\xi_\ell]=\mathrm{i}2\omega F\right\}\mathscr{W}\,\mathrm{d}\Omega, \tag{5.4}$$

where $\mathscr{W}$ is a weighting function to be chosen shortly. By partial integration, and the use of boundary conditions (5.1) and (5.3), the preceding equation becomes

$$\iint_{\Omega_A}\left[\sum_{\ell=0}^{N_\xi}(A_{m,\ell}\nabla\xi_\ell\cdot\nabla\mathscr{W}-B_{m,\ell}\mathscr{W}\nabla h\cdot\nabla\xi_\ell-C_{m,\ell}\xi_\ell\mathscr{W})\right]\mathrm{d}\Omega$$

$$=\int_0^\pi\mathscr{W}A_{m,m}\left(\frac{\partial\xi_m^P}{\partial r}+\frac{\partial\xi_m^H}{\partial r}\right)a\,\mathrm{d}\theta+\iint_{\Omega_A}\mathrm{i}2\omega F\mathscr{W}\mathrm{d}\Omega,\quad m=0,1,2,3,\ldots,N_\xi. \tag{5.5}$$

Use has been made of (3.23) where $A_{\ell,m}$ is diagonal.

Now the domain Ω_A is discretized to an assemblage of three-node triangular elements ($\triangle_e$) with a total of N_E elements and N_P nodes, among which N_B boundary

https://doi.org/10.1017/S0022112005008530 Published online by Cambridge University Press

nodes are designated to be at the end of the sequence, and are labelled as nodes $N_P - N_B + 1$ to N_P. The unknown variable ξ_ℓ is replaced by

$$\xi_\ell = \sum_{n=1}^{N_P} \xi_{\ell,n} \mathscr{W}_n(x, y), \quad \ell = 0, 1, 2, 3, \ldots, \tag{5.6}$$

where $\xi_{\ell,n}$ denotes the nth unknown nodal coefficient of ξ_ℓ and $\mathscr{W}_n$ the global weighting function. In addition, we choose $\mathscr{W}_\tau$ with $\tau = 1, 2, 3, \ldots, N_p$ to be the weighting function $\mathscr{W}$ in (5.5). Accordingly, (5.5) is approximated as

$$\sum_{\ell=0}^{N_\xi} \sum_{n=1}^{N_P} \xi_{\ell,n} \left\{ \sum_{\triangle_e=1}^{N_E} \iint_{\triangle_e} [(A_{m,\ell} \nabla \mathscr{W}_n \cdot \nabla \mathscr{W}_\tau - B_{m,\ell} \mathscr{W}_\tau \nabla h \cdot \nabla \mathscr{W}_n - C_{m,\ell} \mathscr{W}_n \mathscr{W}_\tau)] \, \mathrm{d}\Omega \right\}$$
$$- \int_0^\pi \mathscr{W}_\tau A_{m,m} \frac{\partial \xi_m^H}{\partial r} a \, \mathrm{d}\theta = \int_0^\pi \mathscr{W}_\tau A_{m,m} \frac{\partial \xi_m^P}{\partial r} a \, \mathrm{d}\theta + \sum_{\Omega_e=1}^{N_E} \iint_{\Omega_e} \mathrm{i}2\omega F \mathscr{W}_\tau \, \mathrm{d}\Omega,$$
$$m = 0, 1, 2, \ldots, N_\xi, \quad \tau = 1, 2, \ldots, N_p. \tag{5.7}$$

Furthermore, the Fourier series expansion in the free wave ξ_ℓ^H, (4.23), is truncated after $N_{\widehat{\alpha}} + 1$ terms and also the dummy index m for the Fourier series summation is changed to p. The preceding equation becomes

$$\sum_{\ell=0}^{N_\xi} \sum_{n=1}^{N_P} \xi_{\ell,n} \left\{ \sum_{\triangle_e=1}^{N_E} \iint_{\triangle_e} (A_{m,\ell} \nabla \mathscr{W}_n \cdot \nabla \mathscr{W}_\tau - B_{m,\ell} \mathscr{W}_\tau \nabla h \cdot \nabla \mathscr{W}_n - C_{m,\ell} \mathscr{W}_n \mathscr{W}_\tau) \, \mathrm{d}\Omega \right\}$$
$$- \sum_{p=0}^{N_{\widehat{\alpha}}} \epsilon_p \widehat{\alpha}_{m,p} \left\{ [a\kappa_m A_{m,m} K_p'(\kappa_m a)] \int_0^\pi \mathscr{W}_\tau \cos p\theta \, \mathrm{d}\theta \right\}$$
$$= \mathrm{i}2ka A_{m,m} L_m^M \int_o^\pi \mathscr{W}_\tau [\cos(\theta - \theta_I) \exp(\mathrm{i}2ka \cos(\theta - \theta_I)) + \cos(\theta + \theta_I)$$
$$\times \exp(\mathrm{i}2ka \cos(\theta + \theta_I))] \, \mathrm{d}\theta + \mathrm{i}2ka A_{m,m} \cos\theta_I L_m^N \int_0^\pi \mathscr{W}_\tau \exp(\mathrm{i}2ka \cos\theta_I \cos\theta) \cos\theta \, \mathrm{d}\theta$$
$$+ \sum_{\triangle_e=1}^{N_E} \mathrm{i}2\omega \iint_{\triangle_e} F \mathscr{W}_\tau \, \mathrm{d}\Omega, \quad m = 0, 1, 2, \ldots, N_\xi, \quad \tau = 1, 2, \ldots, N_p, \tag{5.8}$$

after using the expression of ξ_ℓ^P (cf. (4.25)).

Let us introduce the following abbreviations,

$$\mathscr{K}_{\tau,n}^{(m,\ell)} = \sum_{\triangle_e=1}^{N_E} \iint_{\triangle_e} (A_{m,\ell} \nabla \mathscr{W}_n \cdot \nabla \mathscr{W}_\tau - B_{m,\ell} \mathscr{W}_\tau \nabla h \cdot \nabla \mathscr{W}_n - C_{m,\ell} \mathscr{W}_n \mathscr{W}_\tau) \, \mathrm{d}\Omega, \tag{5.9}$$

$$\widehat{\mathscr{K}}_{\tau,p}^{(m,m)} = -\epsilon_p a\kappa_m A_{m,m} K_p'(\kappa_m a) \int_0^\pi \mathscr{W}_\tau \cos p\theta \, \mathrm{d}\theta, \tag{5.10}$$

$$\mathscr{Y}_\tau^{(m)} = \mathrm{i}2ka A_{m,m} L_m^M \int_0^\pi \mathscr{W}_\tau [\cos(\theta - \theta_I) \exp(\mathrm{i}2ka \cos(\theta - \theta_I))$$
$$+ \cos(\theta + \theta_I) \exp(\mathrm{i}2ka \cos(\theta + \theta_I))] \, \mathrm{d}\theta + \mathrm{i}2ka A_{m,m} \cos\theta_I L_m^N$$
$$\times \int_0^\pi \mathscr{W}_\tau \exp(\mathrm{i}2ka \cos\theta_I \cos\theta) \cos\theta \, \mathrm{d}\theta + \sum_{\triangle_e=1}^{N_E} \mathrm{i}2\omega \iint_{\triangle_e} F \mathscr{W}_\tau \, \mathrm{d}\Omega, \tag{5.11}$$

https://doi.org/10.1017/S0022112005008530 Published online by Cambridge University Press

where all the integrals above are evaluated numerically. Equation (5.8) can then be expressed more compactly as

$$\sum_{\ell=0}^{N_\xi}\sum_{n=1}^{N_P}\xi_{\ell,n}\mathscr{K}_{\tau,n}^{(m,\ell)}+\sum_{p=0}^{N_{\widehat{\alpha}}}\widehat{\alpha}_{m,p}\widehat{\mathscr{K}}_{\tau,p}^{(m,m)}=\mathscr{Y}_{\tau}^{(m)},\quad m=0,1,2,\ldots,N_\xi,\quad \tau=1,2,\ldots,N_P. \tag{5.12}$$

Since $m=0,1,\ldots,N_\xi$ and $\tau=1,2,\ldots,N_P$, these constitute $(N_\xi+1)\times N_P$ equations. There are, however, the same number of unknown nodal coefficients plus $(N_\xi+1)\times(N_{\widehat{\alpha}}+1)$ unknown free-wave coefficients $\widehat{\alpha}_{\ell,m}$. The remaining equations are found from the matching condition (5.2) after using (5.6) and (4.23)

$$-\sum_{n=1}^{N_P}\xi_{\ell,n}\mathscr{W}_n+\sum_{p=0}^{N_{\widehat{\alpha}}}\epsilon_p\widehat{\alpha}_{\ell,p}K_p(\kappa_\ell a)\cos p\theta=-\xi_\ell^P-\xi_\ell^Q,\quad \ell=0,1,2,\ldots,N_\xi. \tag{5.13}$$

Let us multiply (5.13) by $[\epsilon_q A_{\ell,\ell}\kappa_\ell a K_q'(\kappa_\ell a)\cos q\theta]$ with $q=0,1,2,\ldots,N_{\widehat{\alpha}}$ and integrate over $(0\leqslant\theta\leqslant\pi)$. Since

$$\int_0^\pi \cos p\theta\cos q\theta\,\mathrm{d}\theta=0\quad\text{when } p\neq q, \tag{5.14}$$

we obtain

$$\left[\sum_{n=1}^{N_P}\check{\mathscr{K}}_{q,n}^{(\ell,\ell)}\xi_{\ell,n}\right]+\widetilde{\mathscr{K}}_{q,q}^{(\ell,\ell)}\widehat{\alpha}_{\ell,q}=\widetilde{\mathscr{Y}}_q^{(\ell)},\quad \ell=0,1,2,\ldots,N_\xi,\quad q=0,1,2,\ldots,N_{\widehat{\alpha}}, \tag{5.15}$$

where

$$\check{\mathscr{K}}_{q,n}^{(\ell,\ell)}=-\epsilon_q A_{\ell,\ell}\kappa_\ell a K_q'(\kappa_\ell a)\int_0^\pi \mathscr{W}_n\cos q\theta\,\mathrm{d}\theta,$$

$$\widetilde{\mathscr{K}}_{q,q}^{(\ell,\ell)}=\epsilon_q^2 A_{\ell,\ell}\kappa_\ell a K_q'(\kappa_\ell a)K_q(\kappa_\ell a)\int_0^\pi\cos^2 q\theta\,\mathrm{d}\theta=\epsilon_q A_{\ell,\ell}\kappa_\ell a K_q'(\kappa_\ell a)K_q(\kappa_\ell a)\pi$$

and

$$\widetilde{\mathscr{Y}}_q^{(\ell)}=-\epsilon_q A_{\ell,\ell}\kappa_\ell a K_q'(\kappa_\ell a)\int_0^\pi\left(\xi_\ell^P+\xi_\ell^Q\right)\cos q\theta\,\mathrm{d}\theta.$$

The integrals $\check{\mathscr{K}}_{q,n}^{(\ell,\ell)}$ and $\widetilde{\mathscr{Y}}_q^{(\ell)}$ can be evaluated numerically.

Combining (5.12) and (5.15), we obtain the global matrix equation

$$\begin{bmatrix}
\mathbb{K}^{(0,0)} & \widehat{\mathbb{K}}^{(0,0)} & \cdots & \mathbb{K}^{(0,\ell)} & [0] & \cdots & \mathbb{K}^{(0,N_\xi)} & [0]\\
\check{\mathbb{K}}^{(0,0)} & \widetilde{\mathbb{K}}^{(0,0)} & \cdots & [0] & [0] & \cdots & [0] & [0]\\
\vdots & \vdots & \cdots & \vdots & \vdots & \cdots & \vdots & \vdots\\
\mathbb{K}^{(\ell,0)} & [0] & \cdots & \mathbb{K}^{(\ell,\ell)} & \widehat{\mathbb{K}}^{(\ell,\ell)} & \cdots & \mathbb{K}^{(\ell,N_\xi)} & [0]\\
[0] & [0] & \cdots & \check{\mathbb{K}}^{(\ell,\ell)} & \widetilde{\mathbb{K}}^{(\ell,\ell)} & \cdots & [0] & [0]\\
\vdots & \vdots & \cdots & \vdots & \vdots & \cdots & \vdots & \vdots\\
\mathbb{K}^{(N_\xi,0)} & [0] & \cdots & \mathbb{K}^{(N_\xi,\ell)} & [0] & \cdots & \mathbb{K}^{(N_\xi,N_\xi)} & \widehat{\mathbb{K}}^{(N_\xi,N_\xi)}\\
[0] & [0] & \cdots & [0] & [0] & \cdots & \check{\mathbb{K}}^{(N_\xi,N_\xi)} & \widetilde{\mathbb{K}}^{(N_\xi,N_\xi)}
\end{bmatrix}
\begin{bmatrix}
\mathscr{X}^{(0)}\\ \widehat{\mathscr{X}}^{(0)}\\ \vdots\\ \mathscr{X}^{(\ell)}\\ \widehat{\mathscr{X}}^{(\ell)}\\ \vdots\\ \mathscr{X}^{(N_\xi)}\\ \widehat{\mathscr{X}}^{(N_\xi)}
\end{bmatrix}=
\begin{bmatrix}
\mathscr{Y}^{(0)}\\ \widetilde{\mathscr{Y}}^{(0)}\\ \vdots\\ \mathscr{Y}^{(m)}\\ \widetilde{\mathscr{Y}}^{(m)}\\ \vdots\\ \mathscr{Y}^{(N_\xi)}\\ \widetilde{\mathscr{Y}}^{(N_\xi)}
\end{bmatrix} \tag{5.16}$$

https://doi.org/10.1017/S0022112005008530 Published online by Cambridge University Press

where the unknown vectors are defined by

$$\mathscr{X}^{(\ell)} = \begin{bmatrix} \xi_{\ell,1} \\ \vdots \\ \xi_{\ell,n} \\ \vdots \\ \xi_{\ell,N_P} \end{bmatrix}, \quad \widehat{\mathscr{X}}^{(\ell)} = \begin{bmatrix} \widehat{\alpha}_{\ell,0} \\ \vdots \\ \widehat{\alpha}_{\ell,q} \\ \vdots \\ \widehat{\alpha}_{\ell,N_{\hat{\alpha}}} \end{bmatrix}, \tag{5.17}$$

and the forcing vectors by

$$\mathscr{Y}^{(m)} = \begin{bmatrix} \mathscr{Y}_1^{(m)} \\ \vdots \\ \mathscr{Y}_\tau^{(m)} \\ \vdots \\ \mathscr{Y}_{N_P}^{(m)} \end{bmatrix}, \quad \widetilde{\mathscr{Y}}^{(m)} = \begin{bmatrix} \widetilde{\mathscr{Y}}_0^{(m)} \\ \vdots \\ \widetilde{\mathscr{Y}}_q^{(m)} \\ \vdots \\ \widetilde{\mathscr{Y}}_{N_{\hat{\alpha}}}^{(m)} \end{bmatrix}. \tag{5.18}$$

The entries for $\mathbb{K}^{(m,\ell)}$, $\widehat{\mathbb{K}}^{(m,\ell)}$ and $\check{\mathbb{K}}^{(\ell,\ell)}$ are $\mathscr{K}_{\tau,n}^{(m,\ell)}$, $\widehat{\mathscr{K}}_{\tau,p}^{(m,\ell)}$ and $\check{\mathscr{K}}_{q,n}^{(\ell,\ell)}$, respectively. The last matrix $\widetilde{\mathbb{K}}^{(\ell,\ell)}$ is diagonal with entries $\widetilde{\mathscr{K}}_{q,q}^{(\ell,\ell)}$. These matrix equations are solved numerically by using the UC Berkeley program *Distributed SuperLU* which is designed for distributed memory parallel processors, using MPI for interprocess communications. In addition, the Domb–Sykes extrapolation scheme is used to limit the number of evanescent modes N_ξ.

In the limit of constant depth everywhere, the above matrix equation can be separated into $N_\xi + 1$ uncoupled matrix equations as follows,

$$\begin{bmatrix} \mathbb{K}^{(m,m)} & \widehat{\mathbb{K}}^{(m,m)} \\ \check{\mathbb{K}}^{(m,m)} & \widetilde{\mathbb{K}}^{(m,m)} \end{bmatrix} \begin{bmatrix} \mathscr{X}^{(m)} \\ \widehat{\mathscr{X}}^{(m)} \end{bmatrix} = \begin{bmatrix} \mathscr{Y}^{(m)} \\ \widetilde{\mathscr{Y}}^{(m)} \end{bmatrix}, \quad m = 0, 1, 2, 3, \ldots, N_\xi. \tag{5.19}$$

Before discussing results from finite-element computations, let us examine a special case of constant depth.

6. Semicircular peninsula on constant depth

6.1. *Analytical solution*

As an application, we consider the limiting case of a semi-circular vertical cylinder (peninsula) of radius a attached to a straight coast. The sea depth is constant everywhere. Now there is no need for finite elements; region Ω_F corresponds to the entire sea. The problem can, of course, be solved by combining the method of images and the three-dimensional methods of Kim & Yue (1989) or of Chau & Eatock Taylor (1992). In addition to providing information on the effects of incidence angles, this example serves to show that the mild-slope-equation approach is a two-dimensional alternative to Chau & Eatock Taylor. The analytical results are also useful as benchmarks for checking the more numerical tasks involving variable bathymetry.

At first order, the scattered wave coefficient in (4.3) is simply

$$\alpha_m = 2\frac{J_m'(ka)}{H_m'(ka)}\cos m\theta_I, \quad m = 0, 1, 2, 3, \ldots. \tag{6.1}$$

https://doi.org/10.1017/S0022112005008530 Published online by Cambridge University Press

At second order, the free wave satisfies the boundary condition on the cylinder

$$\frac{\partial \xi_\ell^H}{\partial r} = -\frac{\partial \xi_\ell^P}{\partial r}, \quad r = a,\ 0 \leqslant \theta \leqslant \pi, \quad \ell = 0, 1, 2, 3 \ldots, \tag{6.2}$$

and along the coast.

Using the partial wave expansions for the plane waves, we rewrite ξ_ℓ^P as

$$\xi_\ell^P = L_\ell^M \sum_{m=0}^{\infty} \epsilon_m \mathrm{i}^m J_m(2kr) 2\cos m\theta_I \cos m\theta + L_\ell^N \sum_{m=0}^{\infty} \epsilon_m \mathrm{i}^m J_m(2kr\cos\theta_I)\cos m\theta, \tag{6.3}$$

where L_ℓ^M and L_ℓ^N are defined in (4.26). Using (4.23) for ξ_ℓ^H and applying (6.2), we obtain

$$\widehat{\alpha}_{\ell,m} = -2\mathrm{i}^m L_\ell^M \frac{J_m'(2ka)}{K_m'(\kappa_\ell a)\kappa_\ell} 2k\cos m\theta_I - \mathrm{i}^m L_\ell^N \frac{J_m'(2ka\cos\theta_I)}{K_m'(\kappa_\ell a)\kappa_\ell} 2k\cos\theta_I. \tag{6.4}$$

It follows that

$$\xi_\ell^H = \sum_{m=0}^{\infty} -\epsilon_m \mathrm{i}^m K_m(\kappa_\ell r)\cos m\theta 2k \left[L_\ell^M \frac{2J_m'(2ka)}{K_m'(\kappa_\ell a)\kappa_\ell} \cos m\theta_I + L_\ell^N \frac{J_m'(2ka\cos\theta_I)}{K_m'(\kappa_\ell a)\kappa_\ell} \cos\theta_I \right]. \tag{6.5}$$

The corresponding potential Φ^H is

$$\Phi^H = \sum_{\ell=0}^{\infty} \frac{\mathrm{i}g}{2\omega} \frac{\cos\kappa_\ell(z+h)}{\cos\kappa_\ell h} \mathrm{e}^{-\mathrm{i}2\omega t} \sum_{m=0}^{\infty} \epsilon_m \mathrm{i}^m K_m(\kappa_\ell r)\cos m\theta \times \left[L_\ell^M \frac{J_m'(2ka)}{K_m'(\kappa_\ell a)\kappa_\ell} 4k\cos m\theta_I + L_\ell^N \frac{J_m'(2ka\cos\theta_I)}{K_m'(\kappa_\ell a)\kappa_\ell} 2k\cos\theta_I \right] + *. \tag{6.6}$$

Together with the analytical formula (4.29) for ξ_ℓ^Q, the amplitude of the second-order displacement $\zeta_2^{(2)}(r,\theta,t)$ (cf. (3.13)) is

$$\eta_{2,2}^{(2)}(r,\theta) = \sum_{\ell=0}^{\infty}\sum_{m=0}^{\infty} \epsilon_m \cos m\theta \left\{ \mathrm{i}^m L_\ell^M 2\cos m\theta_I \left[J_m(2kr) - \frac{2k}{\kappa_\ell} \frac{J_m'(2ka)}{K_m'(\kappa_\ell a)} K_m(\kappa_\ell r) \right] + \mathrm{i}^m L_\ell^N \left[J_m(2kr\cos\theta_I) - \frac{2k\cos\theta_I}{\widehat{\kappa_\ell}} \frac{J_m'(2ka\cos\theta_I)}{K_m'(\kappa_\ell a)} K_m(\kappa_\ell r) \right] + \int_a^{\infty} r_0\,\mathrm{d}r_0 \left[-\mathrm{i}\frac{2\omega \mathscr{Q}_m(r_0)}{A_{\ell,\ell}} \right] K_m(\kappa_\ell r_>) \left[\frac{I_m'(\kappa_\ell a)}{K_m'(\kappa_\ell a)} K_m(\kappa_\ell r_<) - I_m(\kappa_\ell r_<) \right] \right\}. \tag{6.7}$$

Combined with (2.11), the second-order free-surface height is completely determined.

When the incident wave is parallel to the coastline, the problem is identical to a plane wave scattered by a full cylinder in an open sea. (The first-order incident and reflected waves are in the same direction so that their total amplitude is $2A$.) This closed-form solution should be equivalent to the result of Chau & Eatock Taylor (1992). As a check for correctness and accuracy, we have compared our numerical results with earlier works for the case of $\theta_I = 0$, $r/a = 1$, $h/a = 1$, $\omega^2 a/g = 2$, as plotted in figure 3 by Chau & Eatock Taylor (1992). The agreement is excellent (Chen 2005).

https://doi.org/10.1017/S0022112005008530 Published online by Cambridge University Press

m, n	$ka = 0.1$	$ka = 1$	$ka = 0.5$	$ka = 10$
$\theta_I = \pi$	6, 7	10, 11	23, 19	34, 26
$\theta_I = 5\pi/4$	6, 7	10, 11	22, 19	34, 27
$\theta_I = 3\pi/2$	5, 6	10, 10	21, 18	35, 27

TABLE 1. Number of terms (m, n) used in the double series for $\mathcal{Q}$.

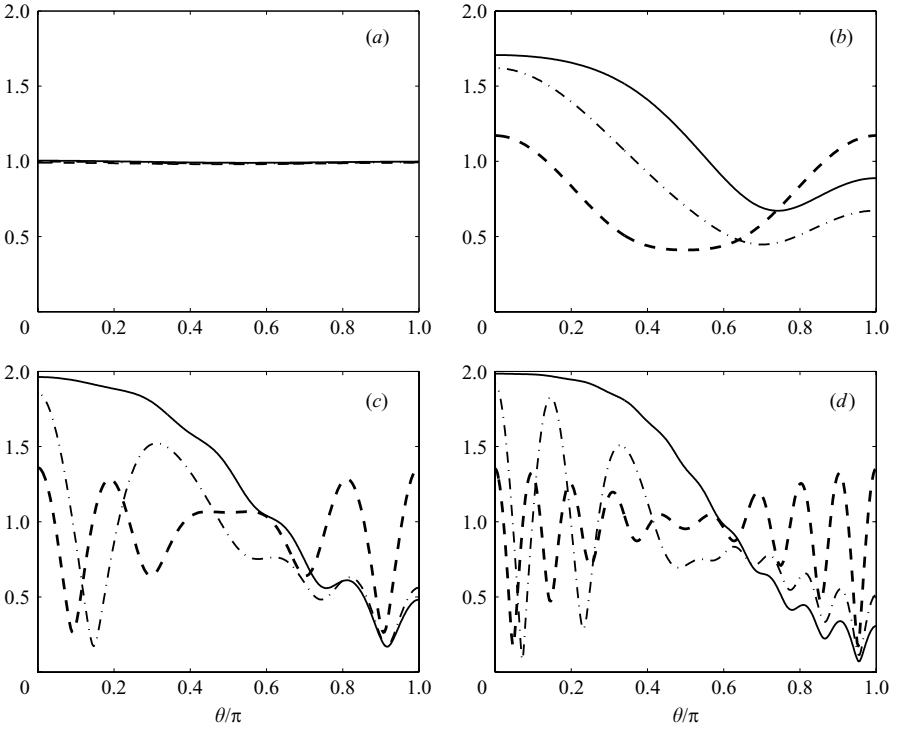


FIGURE 2. Dimensionless amplitudes of first-order $|\eta/A|$ along the semi-circular peninsula for three angles of incidence $\theta_I = \pi$(—), $5\pi/4$ (–·–), $3\pi/2$(– – –), and four cylinder radii: (*a*) $ka = 0.1$, (*b*) $ka = 1$, (*c*) $ka = 5$ and (*d*) $ka = 10$. Depth is fixed $kh = 1$.

6.2. *Effects of incidence angle and cylinder radius*

We have carried out a number of computations to study the effects of incidence angle and the cylinder radius. For brevity only the free-surface displacements (run-up) along the circumference of the cylinder are shown for a fixed depth-to-wavelength ratio $kh = 1$. Three angle of incidences : $\theta_I = \pi$ (glancing), $5\pi/4$ (oblique) and $3\pi/2$ (normal) and four radius-to-wavelength ratios are considered.

In computing the double series of $\mathcal{Q}$ defined in (4.14) and (4.15), both m and n must be truncated after a finite number of terms. These numbers are found by numerical experiments for a fixed error allowance, chosen to be 10^{-5}. As shown in table 1, the numbers increase for larger ka. In addition, the integral for the propagating mode $\ell = 0$ in (6.7) is evaluated by sectioning the integration path. Over one section from a to a finite but large R, numerical integration is performed by the Gaussian three-points adaptive method. In the remaining section from R to ∞, asymptotic approximations are used, as in Chau & Eatock Taylor (1992).

To help understand the second-order results, we first display in figure 2 the first-order run-up along the cylinder. As is well known, for the smallest cylinder $ka = 0.1$,

https://doi.org/10.1017/S0022112005008530 Published online by Cambridge University Press

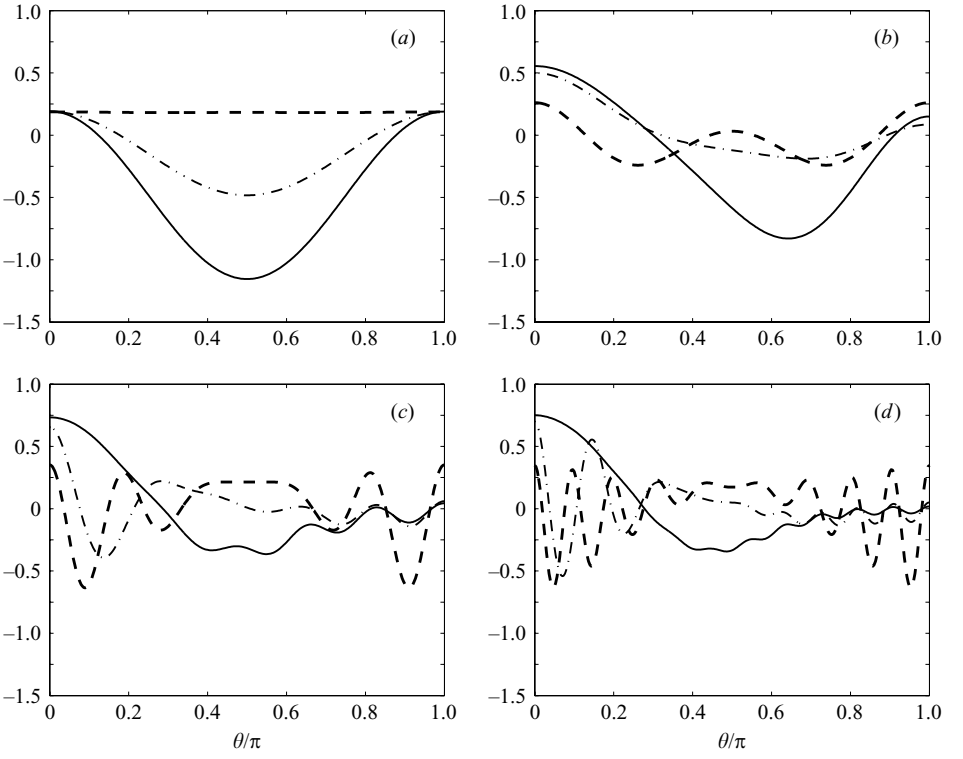


FIGURE 3. Dimensionless amplitudes of second-order $\eta^{(1)}_{2,0}/(4kA^2)$ along the semicircular peninsula, for different angle of incidence $\theta_I = \pi$(—-), $5\pi/4$ (–·–), $3\pi/2$(– – –), and four cylinder radii: (*a*) $ka = 0.1$, (*b*) $ka = 1$, (*c*) $ka = 5$ and (*d*) $ka = 10$. Depth is fixed at $kh = 1$.

the run-up is uniform in all directions, and the effect of incidence angle is small. As the cylinder radius increases relative to the wavelength, the effect of incidence angle becomes more pronounced. For glancing incidence, the runup is the greatest on the incidence side (small θ), and the smallest in the shadow ($\theta \approx \pi$). For normal incidence, the run-up varies strongly in different directions with the greatest run-up at the corners ($\theta = 0, \pi$). The directional variation is oscillatory and symmetrical about the shore-normal axis. With increasing ka, oscillations become more prominent.

The second-order set-up and set-down along the semicircle is shown in figure 3. This quantity is the time-averaged part of the Bernoulli effect on the free surface (cf. (2.10) and (3.10)). For the smallest cylinder, the maximum set-down occurs in the direction $\theta = \pi/2$, being the largest for glancing incidence and smallest for normal incidence. With increasing ka, the set-up and set-down vary with direction in ways similar to the first-order first-harmonic run-up. The largest mean set-up occurs near $\theta = 0$.

The second-harmonic run-up contains two parts (cf. (2.10)). The part due to the first-order interations (cf. (3.12) is shown in figure 4. For glancing incidence, the greatest run-up is at $\theta = \pi/2$ for the smallest cylinder, but near the corner facing the incoming wave for the largest cylinder. For normal incidence, the run-up is oscillatory in θ and symmetrical with respect to the axis $\theta = \pi/2$, similar to the first-order first-harmonic run-up. The part due to second-order potential is shown in figure 5. For glancing incidence, the greatest response appears at $\theta = 0$ for the smallest cylinder, but near

https://doi.org/10.1017/S0022112005008530 Published online by Cambridge University Press

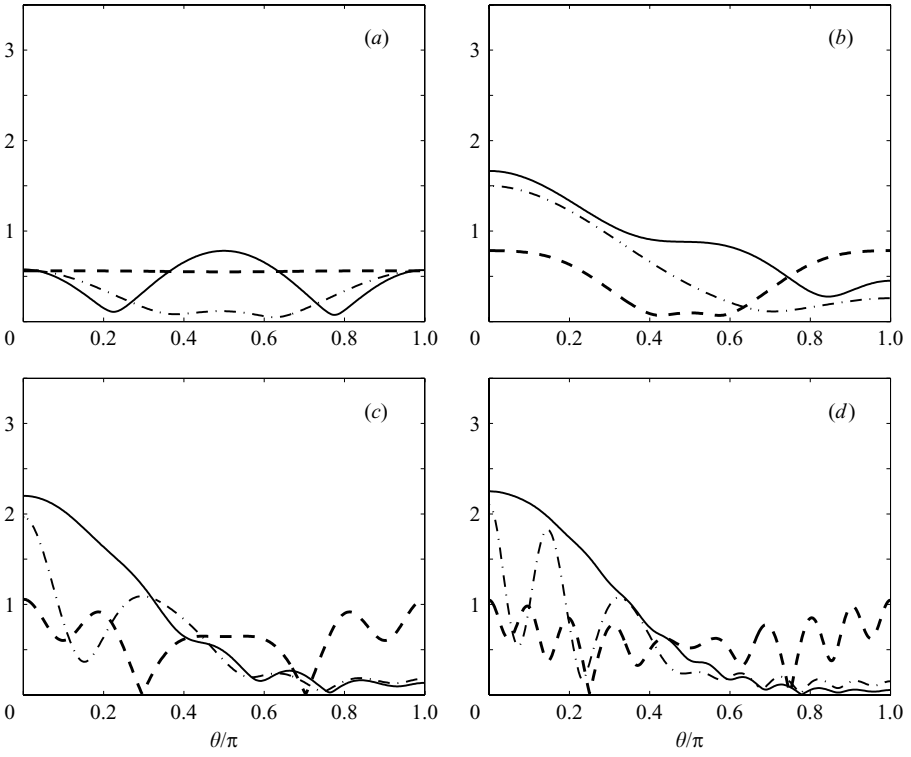


FIGURE 4. As figure 3, but for $|\eta^{(1)}_{2,2}|/(2kA^2)$.

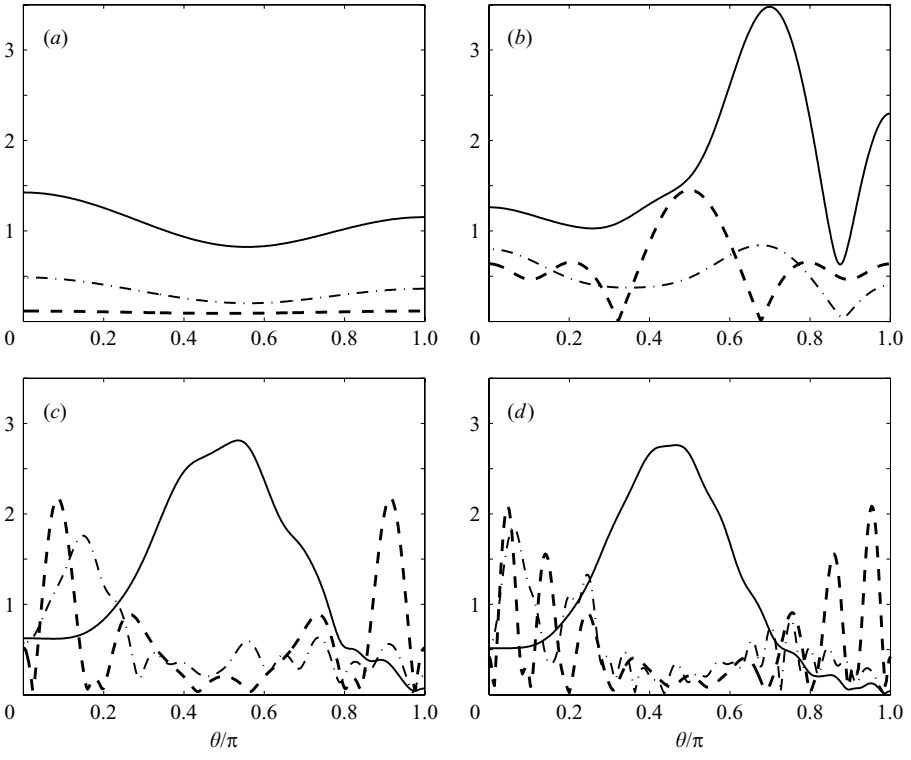


FIGURE 5. As figure 3, but for $|\eta^{(2)}_{2,2}|/(2kA^2)$.

https://doi.org/10.1017/S0022112005008530 Published online by Cambridge University Press

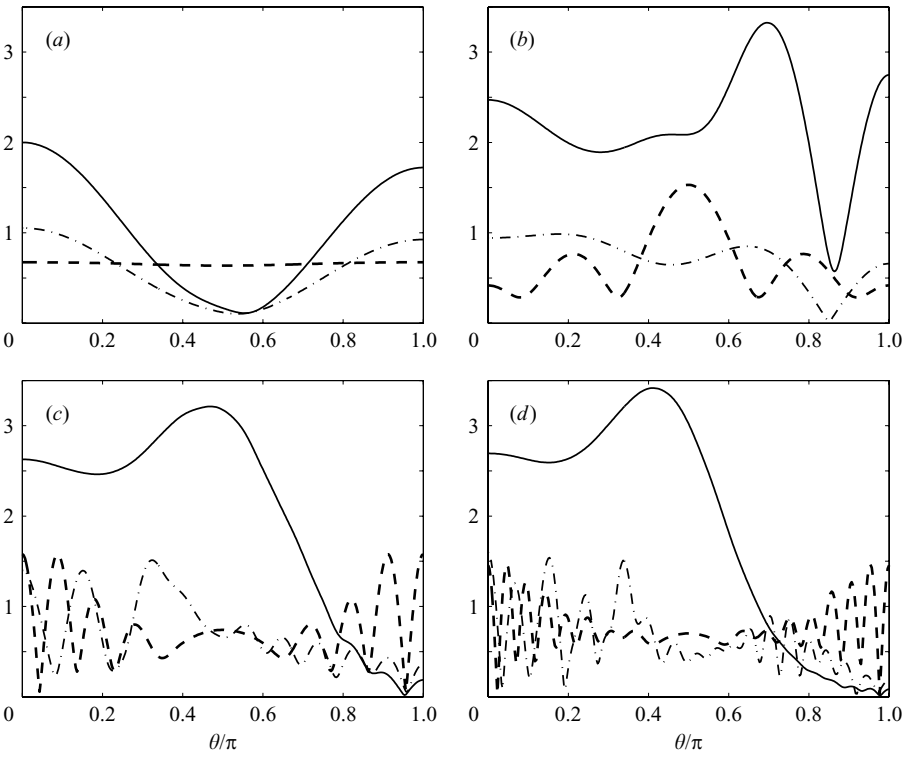


FIGURE 6. As figure 3, but for $|\eta^{(2)}_{2,2} + \eta^{(1)}_{2,2}|/(2kA^2)$.

$\theta = \pi/2$ for the larger cylinders. The total second-harmonic run-up is also shown in figure 6. The relative magnitudes and phases between $\eta^{(1)}_{2,2}$ and $\eta^{(2)}_{2,2}$ depend on θ. The magnitudes of two parts in the total second-harmonic run-up are comparable.

7. A cylinder on top of a semicircular shoal

We now apply the theory for an example combining diffraction and refraction. Consider a semicircular cylinder with radius 20 m standing at the centre of a semicircular shoal next to a straight and cliff-like coast. The top of the shoal is a flat semicircle of radius 20 m at depth 20 m. The sea depth increases monotonically with r until $r = 300$ m, outside of which the surrounding sea has the greater constant depth of 40 m. The radial variation of the sea depth is given by

$$h = \begin{cases} 20\,\text{m}, & r \leqslant 20\,\text{m} \\ 30 - 10\cos\left[\dfrac{\pi}{280}(r-20)\right]\text{m}, & 20\,\text{m} \leqslant r \leqslant 300\,\text{m}. \end{cases} \tag{7.1}$$

The frequency is chosen to be $\omega = 0.6873$ rad s^{-1} such that $kh = 2$ in the open sea where $h = 40$ m. At depth $h = 20$ m the local wavenumber is increased to $kh = 1.1697$. Two incidence angles ($\theta_I = \pi$ (glancing) and $3\pi/2$ (normal)) are considered.

In the hybrid-element scheme, finite elements are used to discretize the shoal, $r < a = 300$ m, $0 < \theta < \pi$, outside which ($\Omega_F : r > 300$ m, $0 < \theta < \pi$) the solution is analytical. Numerical accuracy of the first-order computations depends on the number of finite-element nodes N_P (or the grid size), and the number of angular modes N_α included in the scattered waves. We have tested two finite-element grids: coarse grid with $N_P = 73\,040$ and fine grid with $N_P = 175\,625$. Let $k_0 = 0.05\,\text{m}^{-1}$ denote

https://doi.org/10.1017/S0022112005008530 Published online by Cambridge University Press

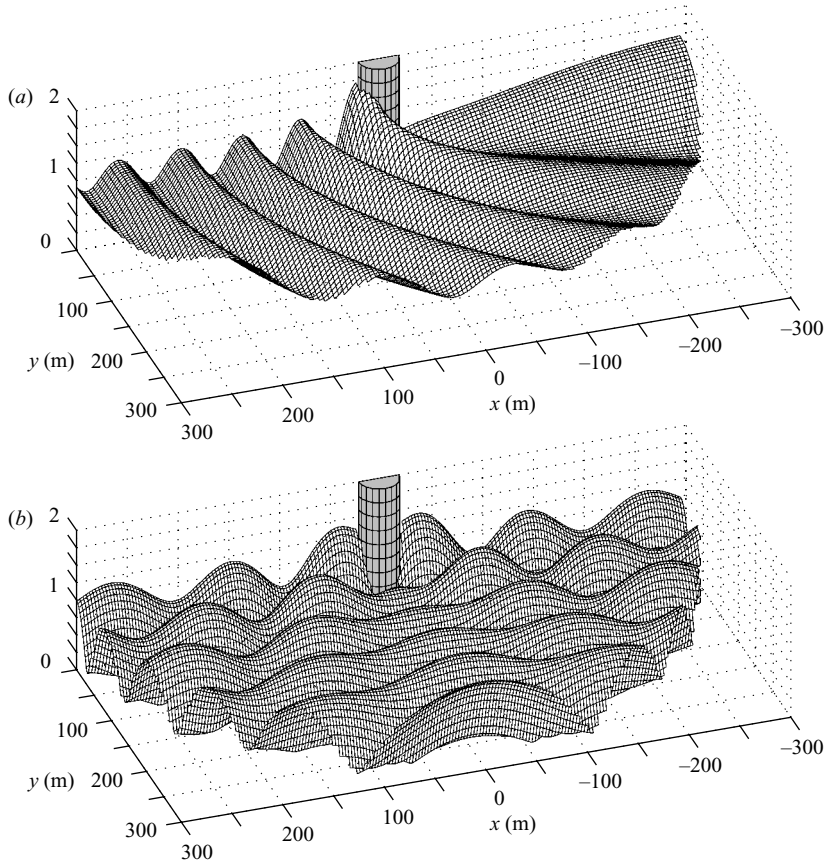


FIGURE 7. The first-order amplitude, $|\eta|/A$, over a semicircular shoal around a cylinder. (a) Glancing incidence. (b) Normal incidence.

the incident wavenumber at $h = 40\,\text{m}$. The maximum element size L_e is such that $k_0 L_e = 0.08$ for the coarse grid, and 0.05 for the fine grid. The corresponding ratios of L_e to wavelength are quite small: 0.012 and 0.008, respectively. For either grid, the solution converges to six decimal places if the number of angular modes is $N_\alpha = 21$ or more. Using 201 angular modes in the outer region, the amplitude for normal incidence at one sample point $\eta(x = 0\,\text{m}, y = 20\,\text{m})/A$ is 0.49802 (coarse) and 0.49824 (fine); the relative error is approximately 4×10^{-4}. Our first-order results are obtained with the fine grid and $N_\alpha = 201$.

For the second-order problems, we use $N_P = 175\,625$ (fine grid) and $N_{\hat{\alpha}} = 91$ (number of angular modes) based on several tests. To limit the number of evanescent modes in the l series, we use the following Domb–Sykes extrapolation scheme. By defining the truncated sum as

$$y^{(l)} = \sum_{\ell=0}^{l} \xi_\ell, \tag{7.2}$$

By plotting $y^{(l)}$ *vs.* $1/l$, the final result is obtained from the limit of $1/l = 0$. Choosing just two values l and $l+1$, the limit by linear extrapolation gives

$$y^{(\infty)} = y^{(l+1)} - l\left[y^{(l)} - y^{(l+1)}\right]. \tag{7.3}$$

https://doi.org/10.1017/S0022112005008530 Published online by Cambridge University Press

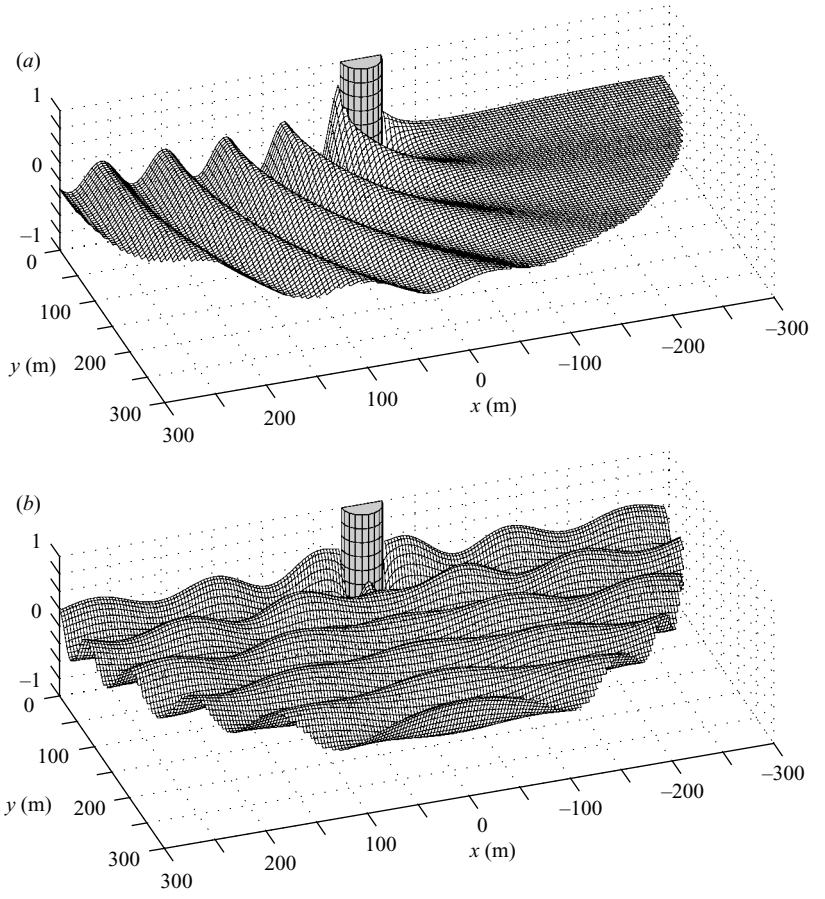


FIGURE 8. The second-order set-down/set-up, $|\eta^{(1)}_{2,0}|/4k_0A^2$, details as figure 7.

We test the number N_ξ of evanescent modes required, based on the numerical results with $l = N_\xi - 1$ and $l + 1 = N_\xi$ in the Domb–Sykes method to extrapolate $y^{(\infty)}$. At the sample point ($x = 20\,\mathrm{m}$, $y = 0\,\mathrm{m}$) the numerical results for $\eta^{(2)}_{2,2}/2kA^2$ are found to be 1.9060 for $N_\xi = 3$ and 1.9117 for $N_\xi = 4$. The complex computer algorithm has been checked satisfactorily with the analytical solution of § 6 by using a ring of finite elements surrounding the peninsula (Chen 2005).

We now discuss the numerical results displayed below only for the shoaling region: $r \leqslant a = 300\,\mathrm{m}$, $0 < \theta < \pi$.

The first-order free-surface amplitudes $|\eta|/A$ for glancing and normal incidences are shown in figure 7. For glancing incidence, the problem is equivalent to a full cylinder on a circular shoal in the open sea, attacked by an incident wave of amplitude $2A$ propagating from left ($x \sim \infty$) to right ($x \sim -\infty$). If the cylinder were absent, the incident rays would enter the shoal first and then bend toward the centre of the shoal; the amplitude would grow slowly towards the orgin. On the lee side, rays would be reflected from the coast and intersect with those incident rays farther away from the coast, resulting in constructive interference and greater amplitude (these features are seen from computed results omitted here). With a cylinder of fairly large radius $k_0a = 1$ where k_0 is the wavenumber at $h = 40\,\mathrm{m}$, strong back-scattering results, as indicated by the wavy envelope in figure 7(*a*). On the shadow side, only a mild increase

https://doi.org/10.1017/S0022112005008530 Published online by Cambridge University Press

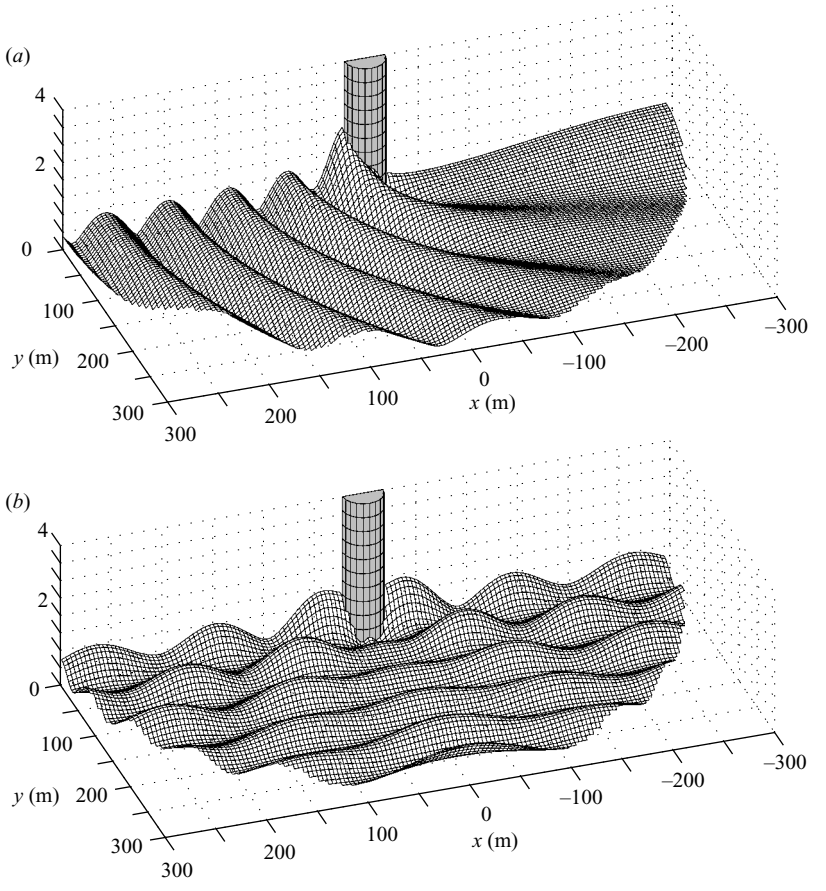


FIGURE 9. The second-harmonic amplitude computed from the first-harmonic, $|\eta^{(1)}_{2,2}|/2k_0A^2$, details as figure 7.

with r is seen owing to the constructive inteference between incident and reflected rays which are not intercepted by the cylinder. All variations gradually diminish far outside the shoal not shown here. For normal incidence without the cylinder, the plot of $|\eta/A|$ would resemble that of a simple standing wave with nodal and antinodal lines parallel to the x-axis. Now scattering from the cylinder adds modulations in all directions as is evident in figure 7(b).

The second-order set-up/set-down of the mean sea level is shown in figure 8 for two incidence angles. Depending solely on the first-order result, the qualitative features resemble those of figure 7. For reference, we recall that the mean sea-level of a progressive wave of amplitude $2A$ on a sea of constant depth is negative and hence a pure set-down $\eta^{(1)}_{20} = -4kA^2/2\sinh 2kh$. On the other hand, the mean sea-level under a simple standing wave over a horizontal seabed is,

$$\eta_{20} = kA^2\left[\frac{\omega^2}{gk}\cos^2 ky - \frac{gk}{\omega^2}\sin^2 ky\right]$$
$$= \frac{kA^2}{2}\frac{1}{\tanh kh}[-(1-\tanh^2 kh) + \cos 2ky(1+\tanh^2 kh)], \qquad (7.4)$$

https://doi.org/10.1017/S0022112005008530 Published online by Cambridge University Press

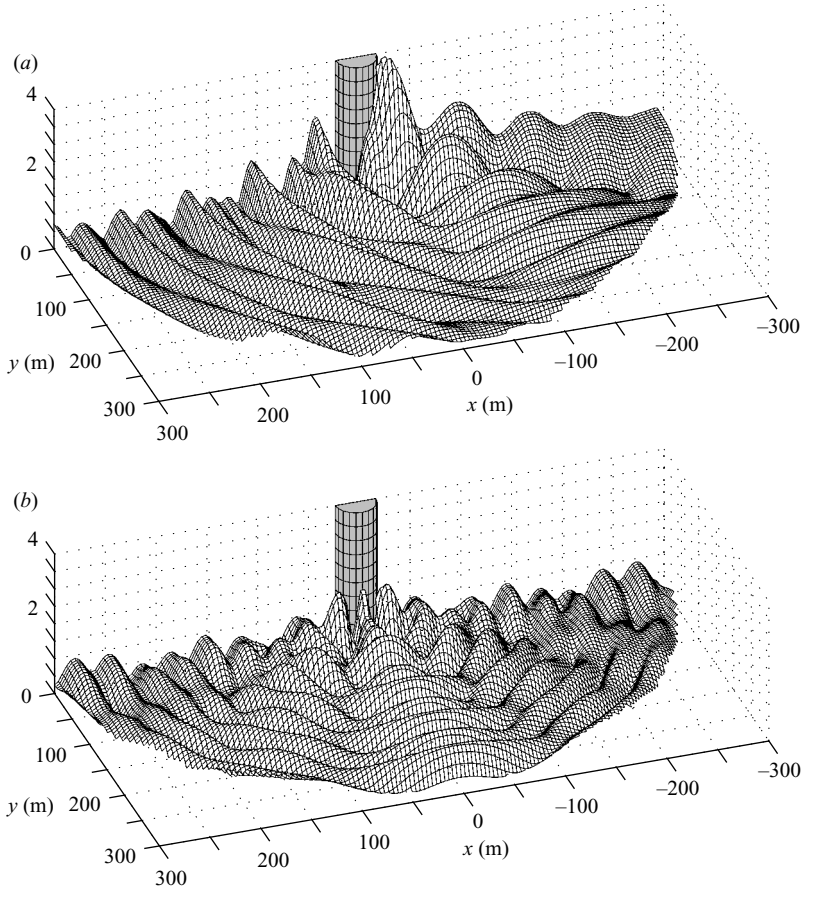


FIGURE 10. The second-order amplitude computed from the second-harmonic, $|\eta^{(2)}_{2,2}|/2k_0A^2$, details as figure 7.

which follows from (3.11) by taking $\eta = A\cos ky$. Unlike the simple progressive, wave, the maximum set-up occurs along the lines $2ky = 0, 2\pi, 4\pi, \ldots$ where $|\eta| = A|\cos ky| = A$ is also the greatest. The maximum set-down occurs at $2kx = \pi, 3\pi, 5\pi, \ldots$, where $|\eta| = A|\cos ky| = 0$ is the smallest. These features are qualitatively preserved in the numerical results, as can be seen from figure 8(*b*). In particular, the mean sea-level along the coast is positive everywhere.

The second-order second-harmonic amplitude has two parts. Figure 9 shows for two incidence angles, $|\eta^{(1)}_{2,2}|/2k_0A^2$ computed from the first-order potential Φ_1. The corresponding maximum amplitude of $\zeta^{(1)}_2$ is $2|\eta^{(1)}_{2,2}|$, hence $2k_0A^2$ is used as the normalizing scale. The variations again resemble those of the first-order amplitude.

Completing the second-order solution is the part $\eta^{(2)}_{2,2}$ associated with Φ_2, shown in figures 10. Note that, for both incidence angles, the spatial undulations are much more rapid, because the characteristic wavenumber is now $\widehat{\kappa}_0$ which is nearly four times the magnitude of k (see (3.21)). As a consequence, the magnitude of the sum of the two complex amplitudes $|\eta^{(1)}_{2,2} + \eta^{(2)}_{2,2}|$ oscillates nearly twice as fast in space, as is shown in figure 11 after accounting for the phases of the two components.

Finally, we compare the free-surface heights along the circumference of two cylinders of the same radius, $r = r_a = 20\,\mathrm{m}$: one on a sea of constant depth (40 m)

https://doi.org/10.1017/S0022112005008530 Published online by Cambridge University Press

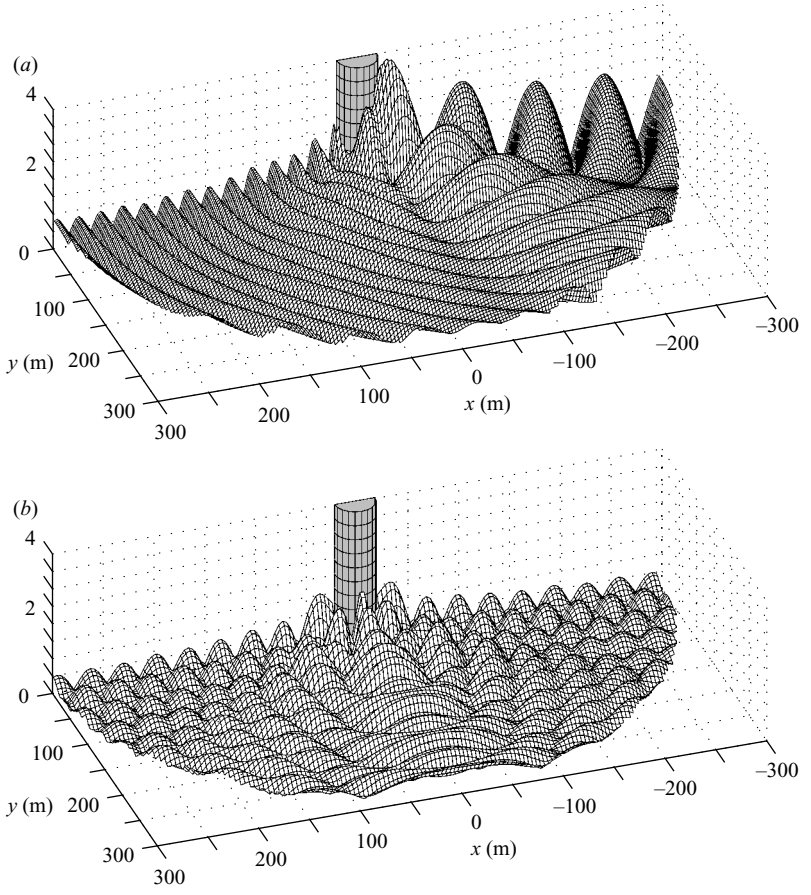


FIGURE 11. The total second-order amplitude, $|\eta^{(1)}_{2,2} + \eta^{(2)}_{2,2}|/2k_0A^2$, details as figure 7.

according to § 6, and the other on top of a shoal just discussed. The incident wave has the same frequency $\omega = 0.6873$ rad s^{-1} so that $k_0h_0 = 2$ in the sea. Note first by comparing figure 12(*a*)–12(*d*) with figures 2(*b*), 3(*b*), 4(*b*), 5(*b*) and 6(*b*) that the results on the cylinder for two different constant depths ($k_0h_0 = 1, 2$) are qualtitatively similar; this is probably because the value of $k_0r_a = 1$ is the same in both examples. Secondly, for both incidence angles, shoaling tends to increase mildly the first-order amplitude $|\eta|$ as well as $|\eta^{(1)}_{2,2}|$, but to decrease the mean sea-level $|\eta^{(1)}_{2,0}|$, all of which depend solely on the first order. However, the part $|\eta^{(2)}_{2,2}|$ is considerably more enhanced by shoaling.

8. Concluding remarks

We have extended the ideas behind the mild-slope equation, developed previously for linearized problems of water-wave diffraction and refraction, to account for nonlinearity up to second order in wave steepness. In the case of uniform depth, the second-order diffraction is governed by a set of uncoupled two-dimensional Helmholtz equations with forcing. An analytical solution is given for a semi-circular peninsula. A hybrid-element method is described for the second-order refraction/diffraction over a slowly varying bathymetry. Numerical results are demonstrated for the diffraction of a cylinder resting on top of a semi-circular shoal. Applications have been made

https://doi.org/10.1017/S0022112005008530 Published online by Cambridge University Press

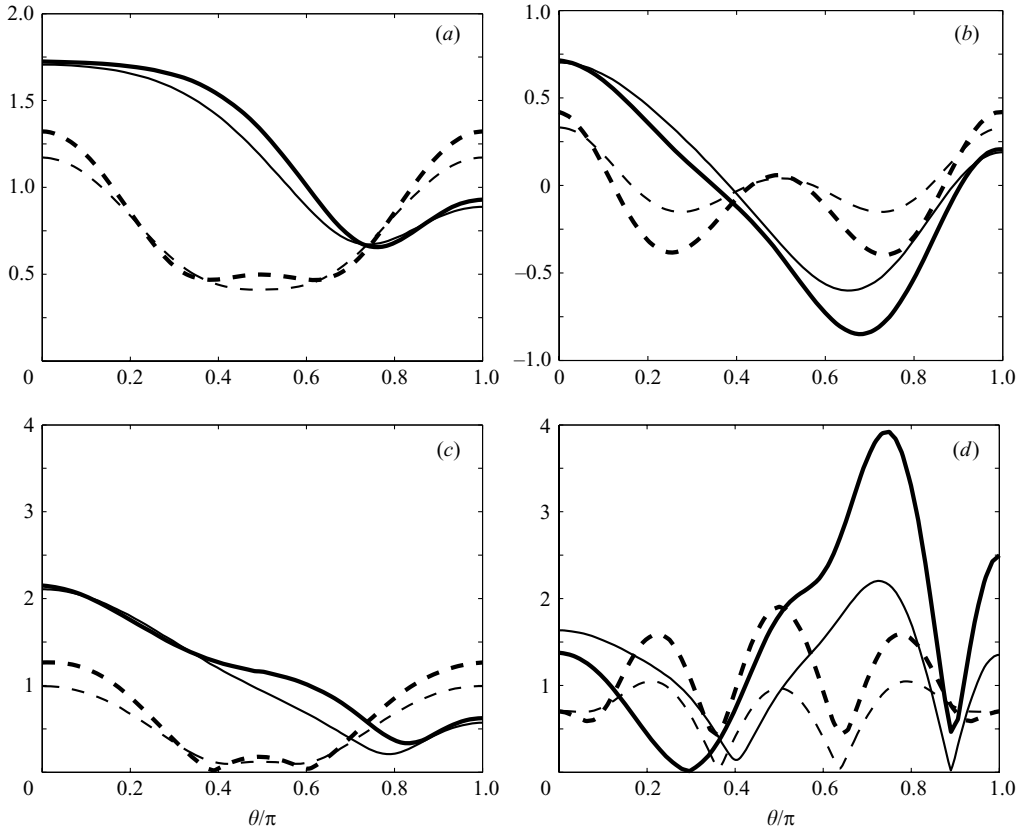


FIGURE 12. Free-surface heights along the semi-circular cylinder of the same radius attacked by an incident wave of the same frequency. For incident wave in deeper water : $k_0h_0 = 2$. Thick lines are for variable depth, $h = h(r)$ varying from 40 m to 20 m. Thin lines are for constant depth $h = h_0 = 40$ m. Solid lines (—): glancing incidence ($\theta_I = \pi$). Dashed lines (– – –): normal incidence ($\theta_I = 3\pi/2$). (*a*) $|\eta|/A$, (*b*) $|\eta^{(1)}_{2,0}|/(4k_0A^2)$, (*c*) $|\eta^{(1)}_{2,2}|/(2k_0A^2)$, (*d*) $|\eta^{(2)}_{2,2}|/(2k_0A^2)$.

to other geometries such as pure shoaling without a scatterer and a harbour behind a shoal (Chen 2005). In past studies, the phenomenon of ringing near an offshore tower has been attributed to third-order effects (Faltinsen, Newman & Vinje 1995). The ideas here can, in principle, be extended to third-order analysis for a tower on a slowly varying seabed, with of course increased algebraic and numerical complexity. Nevertheless, the advantage of this approach that discrete computations are required only for two horizontal coordinates, would probably be even more preferable since refraction usually involves a large domain extending over many wavelengths in all horizontal directions. The fully three-dimensional alternative via either boundary elements or finite elements covering the entire region of variable boundary and bathymetry would appear to be extremely cumbersome and demanding. On the other hand, extending the three-dimensional treatment of Yue *et al.* (1978) and Kim & Yue (1989) only near the structure, and matching with the quasi-two-dimensional mild-slope approximation for the much larger zone of variable depth, may simplify the numerical task considerably.

We point out that the present theory is an extension of Stokes approximation, which is inherently limited to a small Ursell–Stokes parameter ($A/k^2h^3 \ll 1$). For very

https://doi.org/10.1017/S0022112005008530 Published online by Cambridge University Press

shallow water waves propagating over long distances, we must use Boussinesq or other appropriate approximations expressly devised for small kh.

Finally, for treating slow-drift motions of floating platforms or long-period oscillations in harbours, it is necessary to consider nonlinear effects due to random incident waves of broad frequency band. The present theory can be extended to facilitate the analysis, as will be reported in the near future.

The authors thank the US Office of Naval Research (Grant N00014-04-1-0077), US National Science Foundation (Grant CTS-0075713) and the US–Israel Binational Science Foundation (Grant 200405) for their financial support of this study.

Appendix A. Derivation of second-order mild-slope equation

We outline the derivation by following the procedure of Smith & Sprinks (1975) for the linearized homogeneous problem with the frequency ω. Except for the inhomogeneous term, and the change of frequency to 2ω, the result is similar to that of Porter & Staziker (1995) derived by a different method for the first-order problem.

The function $\psi(x, y, z)$ satisfies

$$\nabla^2\psi + \frac{\partial^2\psi}{\partial z^2} = 0, \quad -h(x, y) < z < 0, \tag{A 1}$$

$$\frac{\partial\psi}{\partial z} = -\nabla\psi\cdot\nabla h, \quad z = -h(x, y), \tag{A 2}$$

$$\frac{\partial\psi}{\partial z} - \frac{4\omega^2}{g}\psi = F, \quad z = 0. \tag{A 3}$$

Let us introduce

$$f_m = \frac{\cos\kappa_m(z+h)}{\cos\kappa_m h} \tag{A 4}$$

which satisfies

$$\frac{\partial^2 f_m}{\partial z^2} + \kappa_m^2 f_m = 0, \quad -h < z < 0, \tag{A 5}$$

$$\frac{\partial f_m}{\partial z} = 0, \quad z = -h, \tag{A 6}$$

$$\frac{\partial f_m}{\partial z} - \frac{4\omega^2}{g} f_m = 0, \quad z = 0, \tag{A 7}$$

where κ_m, $m = 0, 1, 2, \ldots$ are defined by (3.20) and $\kappa_o = -\mathrm{i}\widehat{\kappa}_0$ is defined by (3.21).

Regarding (A 1) as an ordinary differential equation in z and applying Green's formula to f_m and ψ, we obtain, after using (A 1)–(A 7),

$$\int_{-h}^{0} \left(-\psi\kappa_m^2 f_m + f_m\nabla^2\psi\right) \mathrm{d}z = -(f_m)_{z=0}\, F - (f_m\nabla\psi\cdot\nabla h)_{z=-h}\,. \tag{A 8}$$

With the assumption,

$$\psi = -\frac{\mathrm{i}g}{2\omega}\sum_{\ell=0}^{\infty}\xi_\ell(x, y) f_\ell(x, y, z), \tag{A 9}$$

https://doi.org/10.1017/S0022112005008530 Published online by Cambridge University Press

(A 8) becomes

$$\sum_{\ell=0}^{\infty}\left\{-\xi_\ell\kappa_m^2 g\int_{-h}^{0} f_m f_\ell\,\mathrm{d}z+\xi_\ell g\int_{-h}^{0} f_m\frac{\partial f_\ell}{\partial h}\nabla^2\,\mathrm{d}z+\xi_\ell g\int_{-h}^{0} f_m\frac{\partial^2 f_\ell}{\partial h^2}(\nabla h)^2\,\mathrm{d}z\right.$$
$$\left.+(\nabla^2\xi_\ell)g\int_{-h}^{0} f_m f_\ell\,\mathrm{d}z+(\nabla\xi_\ell)\cdot\left(g\int_{-h}^{0} 2f_m\frac{\partial f_\ell}{\partial h}\nabla h\,dz\right)\right\}$$
$$=-2\mathrm{i}\omega F-\sum_{\ell=0}^{\infty}\left\{\left[\xi_\ell g f_m\frac{\partial f_\ell}{\partial h}(\nabla h)^2+(\nabla\xi_\ell)\cdot(g f_m f_\ell\nabla h)\right]_{z=-h}\right\}. \tag{A 10}$$

After using Leibniz' rule,

$$\nabla\cdot\left(\int_{-h}^{0} f_m f_\ell\nabla\xi_\ell dz\right)=\int_{-h}^{0} f_m f_\ell\nabla^2\xi_\ell\,\mathrm{d}z+\int_{-h}^{0} f_m\frac{\partial f_\ell}{\partial h}\nabla h\cdot\nabla\xi_\ell\,\mathrm{d}z$$
$$+\int_{-h}^{0} f_\ell\frac{\partial f_m}{\partial h}\nabla h\cdot\nabla\xi_\ell\,dz+(f_\ell f_m\nabla\xi_\ell\cdot\nabla h)_{z=-h}, \tag{A 11}$$

(A 10) can be written as

$$\sum_{\ell=0}^{\infty}\left\{\xi_\ell\left(-\kappa_m^2 g\int_{-h}^{0} f_m f_\ell\,\mathrm{d}z\right)+\nabla\cdot\left[(\nabla\xi_\ell)\left(g\int_{-h}^{0} f_m f_\ell\,\mathrm{d}z\right)\right]\right.$$
$$+\int_{-h}^{0} g\left(f_m\frac{\partial f_\ell}{\partial h}-f_\ell\frac{\partial f_m}{\partial h}\right)\nabla h\cdot\nabla\xi_\ell\,\mathrm{d}z+\int_{-h}^{0} g f_m\frac{\partial f_\ell}{\partial h}\xi_\ell\nabla^2 h$$
$$\left.+\int_{-h}^{0} g f_m\xi_\ell\frac{\partial^2 f_\ell}{\partial h^2}(\nabla h)^2\,\mathrm{d}z+g\left[f_m\xi_\ell\frac{\partial f_\ell}{\partial h}(\nabla h)^2\right]_{z=-h}\right\}=-\mathrm{i}2\omega F. \tag{A 12}$$

Equation (A 12) can be simplified to the form

$$\sum_{\ell=0}^{\infty}\{\nabla\cdot(A_{m,\ell}\nabla\xi_\ell)+B_{m,\ell}\nabla h\cdot\nabla\xi_\ell+C_{m,\ell}\xi_\ell\}=-\mathrm{i}2\omega F \tag{A 13}$$

where

$$A_{m,\ell}=g\int_{-h}^{0}(f_m f_\ell)\,\mathrm{d}z, \tag{A 14}$$
$$B_{m,\ell}=g(U_{m,\ell}-U_{\ell,m}), \tag{A 15}$$
$$U_{m,\ell}=\int_{-h}^{0}\left(f_m\frac{\partial f_\ell}{\partial h}\right)\mathrm{d}z, \tag{A 16}$$
$$C_{m,\ell}=-\kappa_m^2 A_{m,\ell}+g U_{m,\ell}\nabla^2 h+g V_{m,\ell}\,(\nabla h)^2 \tag{A 17}$$

and

$$V_{m,\ell}=\int_{-h}^{0}\left(f_m\frac{\partial^2 f_\ell}{\partial h^2}\right)\mathrm{d}z+\left[f_m\frac{\partial f_\ell}{\partial h}\right]_{z=-h}. \tag{A 18}$$

Using Leibniz' rule, we can rewrite $V_{m,\ell}$ as

$$V_{m,\ell}=\frac{\partial}{\partial h}\int_{-h}^{0}\left(f_m\frac{\partial f_\ell}{\partial h}\right)\mathrm{d}z-\int_{-h}^{0}\left(\frac{\partial f_m}{\partial h}\frac{\partial f_\ell}{\partial h}\right)\mathrm{d}z$$
$$=\frac{\partial U_{m,\ell}}{\partial h}-\int_{-h}^{0}\left(\frac{\partial f_m}{\partial h}\frac{\partial f_\ell}{\partial h}\right)\mathrm{d}z. \tag{A 19}$$

https://doi.org/10.1017/S0022112005008530 Published online by Cambridge University Press

By using the orthogonality of the vertical eigenfunctions $\{f_m\}$, $A_{m,\ell}$ is found as given by (3.23). After straightforward but lengthy algebra (Chen 2005), we obtain the coefficients given explicitly by (3.25) to (3.28).

Appendix B. Equivalence to Stokes waves

We show here that (4.27) and (4.28) are equivalent to Stokes waves of the following standard form:

$$\begin{pmatrix}\Phi_2^I\\ \Phi_2^R\end{pmatrix}_{Stokes} = -\frac{3\mathrm{i}\omega}{4}\frac{\cosh 2k\,(z+h)}{\sinh^4 kh}\frac{A^2}{4}\exp(\mathrm{i}2kr\cos(\theta \mp \theta_I) - 2\mathrm{i}\omega t) + *, \tag{B 1}$$

$$\begin{aligned}\left(\Phi_2^{IR}\right)_{Stokes} = &-\frac{\mathrm{i}A^2\omega}{2g}\frac{1+2\cos 2\theta_I - 3\tanh^2 kh}{\tanh kh\,[2\cos\theta_I \tanh(2kh\cos\theta_I) - 4\tanh kh]}\\ &\times\frac{\cosh[2k(z+h)\cos\theta_I]}{\cosh(2kh\cos\theta_I)}\exp(\mathrm{i}2kr\cos\theta_I\cos\theta - 2\mathrm{i}\omega t) + *.\end{aligned} \tag{B 2}$$

To show this, we first obtain from (3.16),

$$\widehat{\beta} - \bar{\beta}k^2 = \frac{3\omega k}{\sinh kh\cosh kh}, \quad \widehat{\beta} - \bar{\beta}k^2\cos(2\theta_I) = \frac{\mathrm{i}k\omega}{\tanh kh}[1 + 2\cos(2\theta_I) - 3\tanh^2 kh]. \tag{B 3}$$

The Stokes wave potential can be rewritten as

$$\begin{aligned}\begin{pmatrix}\Phi_2^I\\ \Phi_2^R\end{pmatrix}_{Stokes} = &-\left[\frac{\cosh kh}{4k\sinh^3 kh}\cosh 2k\,(z+h)\right]\\ &\times(\widehat{\beta} - \bar{\beta}k^2)\frac{A^2}{4}\exp(\mathrm{i}2kr\cos(\theta - \theta_I) - 2\mathrm{i}\omega t) + *,\end{aligned} \tag{B 4}$$

$$\begin{aligned}(\Phi_2^{IR})_{Stokes} = &-\frac{\mathrm{i}A^2\omega}{2g}\frac{\widehat{\beta} - \bar{\beta}k^2\cos(2\theta_I)}{[2\cos\theta_I\tanh(2kh\cos\theta_I) - 4\tanh kh]}\\ &\times\frac{\cosh[2k(z+h)\cos\theta_I]}{\cosh(2kh\cos\theta_I)}\exp(\mathrm{i}2kr\cos\theta_I\cos\theta - 2i\omega t) + *.\end{aligned} \tag{B 5}$$

Let us expand $\cosh 2k(z+h)$ and $\cosh[2k(z+h)\cos\theta_I]$ in terms of the vertical eigenfunctions

$$\cosh 2k\,(z+h) = \sum_{\ell=0}^{\infty} a_\ell f_\ell, \qquad \cosh[2k(z+h)\cos\theta_I] = \sum_{\ell=0}^{\infty} b_\ell f_\ell, \tag{B 6}$$

where

$$f_\ell = \frac{\cos k_\ell\,(z+h)}{\cos\kappa_\ell h}. \tag{B 7}$$

By using the orthogonality of f_ℓ, the dispersion relation as well as the identities

$$2\tanh 2kh - 4\tanh kh = -\frac{4\sinh^3 kh}{\cosh kh\cosh 2kh}, \qquad \kappa_\ell\tan\kappa_\ell h = -\frac{4\omega^2}{g} = -4k\tanh kh, \tag{B 8}$$

we obtain

$$a_\ell = -\frac{g}{A_{\ell,\ell}}\frac{4k\sinh^3 kh}{\cosh kh}\frac{1}{4k^2+\kappa_\ell^2}, \tag{B 9}$$

https://doi.org/10.1017/S0022112005008530 Published online by Cambridge University Press

$$b_\ell = -\frac{g}{A_{\ell,\ell}} \frac{[2k\cos\theta_I \tanh(2kh\cos\theta_I) - 4k\tanh kh]\cosh(2kh\cos\theta_I)}{(4k^2+\kappa_\ell^2)}, \tag{B 10}$$

where $A_{\ell,\ell}$ is given by (3.23). The equivalence of (B 4) and (4.27) and of (B 5) and (4.28) is evident.

Appendix C. Two-dimensional Green's function

We define the Green function by

$$\nabla^2 G_\ell - \kappa_\ell^2 G_\ell = \frac{1}{r}\delta(r-r_0)\left[\delta(\theta-\theta_0)+\delta(\theta+\theta_0)\right], \quad r, r_0 > a, \tag{C 1}$$

$$\frac{\partial G_\ell}{\partial \theta} = 0, \quad \theta = 0,\ \pi, \tag{C 2}$$

$$\frac{\partial G_\ell}{\partial r} = 0, \quad r = a. \tag{C 3}$$

For the propagating mode $\ell = 0$, the usual (strong) radiation condition is required,

$$\sqrt{r}\left(\frac{\partial G_0}{\partial r} - \mathrm{i}\widehat{\kappa}_0 G_0\right) \to 0, \quad r \to \infty. \tag{C 4}$$

For the evanescent modes $\ell = 1, 2, 3, \ldots$, we require that

$$G_\ell \to 0, \quad r \to \infty, \quad \ell = 1, 2, 3, \ldots. \tag{C 5}$$

By the standard method of eigenfunction expansions, we obtain the following result,

$$G_\ell = \frac{1}{\pi}\sum_{m=0}^{\infty} \epsilon_m g_{\ell m} \cos m\theta \cos m\theta_0 \tag{C 6}$$

where

$$g_{\ell m}(r, r_0) = \left[\frac{I_m'(\kappa_\ell a)}{K_m'(\kappa_\ell a)} K_m(\kappa_\ell r_0) - I_m(\kappa_\ell r_0)\right] K_m(\kappa_\ell r), \quad r > r_0, \tag{C 7}$$

and

$$g_{\ell m}(r, r_0) = \left[\frac{I_m'(\kappa_\ell a)}{K_m'(\kappa_\ell a)} K_m(\kappa_\ell r) - I_m(\kappa_\ell r)\right] K_m(\kappa_\ell r_0), \quad r < r_0. \tag{C 8}$$

Clearly, the Green function is symmetric: $G_\ell(r, \theta; r_0, \theta_0) = G_\ell(r_0, \theta_0; r, \theta)$. Defining

$$r_> = \mathrm{Max}(r, r_0), \quad r_< = \mathrm{Min}(r, r_0), \tag{C 9}$$

we express the Green function in a more compact form,

$$G_\ell(r_>, r_<) = \sum_{m=0}^{\infty} \frac{\epsilon_\ell}{\pi}\left[\frac{I_m'(\kappa_\ell a)}{K_m'(\kappa_\ell a)} K_m(\kappa_\ell r_<) - I_m(\kappa_\ell r_<)\right] K_m(\kappa_\ell r_>)\cos m\theta \cos m\theta_0. \tag{C 10}$$

REFERENCES

Agnon, Y. 1999 Linear and nonlinear refraction and bragg scattering of water waves. *Phys. Rev.* E **59**, R1319–1322.

Athanassoulis, G. A. & Belibassakis, K. A. 1999 A consistent coupled-mode theory for the propagation of small-amplitude water waves over variable bathymetry regions. *J. Fluid Mech.* **389**, 275–301.

https://doi.org/10.1017/S0022112005008530 Published online by Cambridge University Press

Bai, K. J. & Yeung, R. 1974 Numerical solutions of free-surface and flow problems. *Proc. 10th Symp. Naval Hydrodyn., Office of Naval Research*, pp. 609–641.

Berkhoff, J. C. W. 1972 Computation of combined refraction–diffraction. *Proc. 13th Conf. Coastal Engng ASCE*, vol. 1, pp. 471–490.

Chamberlain, P. G. & Porter, D. 1995 The modified mild-slope equation. *J. Fluid Mech.* **291**, 393–407.

Chau, F. P. & Eatock Taylor, R. 1992 Second-order wave diffraction by a vertical cylinder. *J. Fluid Mech.* **240**, 571–599.

Chen, H. S. & Mei, C. C. 1974 Oscillations and wave forces in a man-made harbor in the open sea. *Proc. 10th Symp. Naval Hydrodyn.* pp. 573–594.

Chen, M.-Y. 2005 Nonlinear refraction and diffraction of regular and random waves. PhD thesis, Dept of Civil & Environmental Engineering, MIT.

Faltinsen, O. M., Newman, J. N. & Vinje, T. 1995 Nonlinear wave loads on a slender vertical cylinder. *J. Fluid Mech* **289**, 179–198.

Houston, J. R. 1981 Combined refraction and diffraction of short waves using the finite element method. *Appl. Ocean Res.* **3** (4), 163–170.

Kim, M.-H. & Yue, D. K. P. 1989 The complete second-order diffraction solution for an axisymmetric body. Part 1. Monochromatic incident waves. *J. Fluid Mech.* **200**, 235–264.

Kirby, J. T. 1986 A general wave equation for waves over rippled beds. *J. Fluid Mech*. **162**, 171–186.

Longuet-Higgins, M. S. 1950 The theory of the origin of microseisms. *Phil. Trans. R. Soc. Lond*. A **243**, 1–35.

Massel, S. R. 1993 Extended refraction–diffraction equation for surface waves. *Coastal Engng*. **19**, 97–126.

Mei, C. C. 1989 *The Applied Dynamics of Ocean Surface Waves*. World Scientific.

Miles, J. W. & Chamberlain, P. G. 1998 Topographical scattering of gravity waves. *J. Fluid Mech*. **361**, 175–188.

Porter, D. & Staziker, D. J. 1995 Extensions of the mild-slope equation. *J. Fluid Mech.* **300**, 367–382.

Smith, R. & Sprinks, T. 1975 Scattering of surface waves by a conical island. *J. Fluid Mech.* **72**, 373–384.

Yue, D. K. P., Chen, H. S. & Mei, C. C. 1978 A hybrid element method for diffraction of water waves by three-dimensional bodies. *Intl. J. Numer. Meth. Engng.* **12**, 245–266.

https://doi.org/10.1017/S0022112005008530 Published online by Cambridge University Press